Combustion and Flame

A ReaxFF molecular dynamics study of polycyclic aromatic hydrocarbon oxidation assisted by nitrogen oxides

--Manuscript Draft--

Manuscript Number:	CNF-D-22-00606R3
Article Type:	Full Length Article
Keywords:	PAHs; Nitrogen oxides; Oxidation; Reaxff; Molecular dynamics simulation
Corresponding Author:	Qian Mao RWTH Aachen University Aachen, GERMANY
First Author:	Ying Wang
Order of Authors:	Ying Wang
	Qian Mao
	Zhanyuan Wang
	Kai H. Luo
	Lei Zhou
	Haiqiao Wei
Abstract:	Fossil fuel-derived soot poses a persistent problem. A joint reduction is conducted via the reaction between NOx and soot. The underlying reaction mechanisms of large polycyclic aromatic hydrocarbons (PAHs), as well as the interactions between O2, NO and NO2, have been extensively investigated by ReaxFF molecular dynamics simulations for the first time. The pyrolysis and oxidation of coronene are conducted at 2500 K and 50 atm. Coronene in the pyrolysis system first experiences dehydrogenation reactions and subsequently undergoes recombination reactions, leading to the formation of large PAHs. Among the three oxidizers, NO2 is the strongest in coronene oxidation, followed by NO and O2. Meanwhile, the O radical is identified as the key species for PAH oxidation. In the presence of O2, the formation of O radicals requires the assistance of H radicals that are formed by the dehydrogenation of PAHs, which retards the oxidation process. In the presence of NO, O radicals can be directly formed via reactions of NO → N + O and N + NO ⇌ N2 + O. NO2 first undergoes a decomposition reaction: NO2 → NO + O, followed by NO decomposition. O-addition and N-addition, as well as subsequent fragmentation reactions including the generation of COx and (H)CN are important routes in PAH oxidation. Furthermore, compared to NO, NO2 provides more O radicals that significantly accelerate PAH oxidation. This study provides fundamental insight into PAH oxidation that may help to design strategies to inhibit soot and NOx emissions at the source.

Dear Editor of Combustion and Flame:

We would like to submit the enclosed manuscript entitled "**A ReaxFF molecular dynamics study of polycyclic aromatic hydrocarbon oxidation assisted by nitrogen oxides**". The current manuscript is approved by all authors for publication. I would like to declare on behalf of my co-authors that the work described was original research that has not been published previously.

The major objective of the present study is to investigate the reaction mechanisms of large PAH pyrolysis and oxidation at high temperature and pressure condition by using the ReaxFF molecular dynamics (MD) simulations. The present study emphasizes the reaction routes of large PAH oxidation by NO and NO_2 from the atomistic perspective. Detailed insight into the key reactive events related to pyrolysis and oxidation of PAHs will not only facilitate our understanding of combustion chemistry but also be helpful in developing comprehensive kinetic models.

We deeply appreciate your consideration of our manuscript and please accept it as a candidate for publication in Combustion and Flame.

Sincerely,

Faithfully yours,

Qian Mao

Graphical abstract

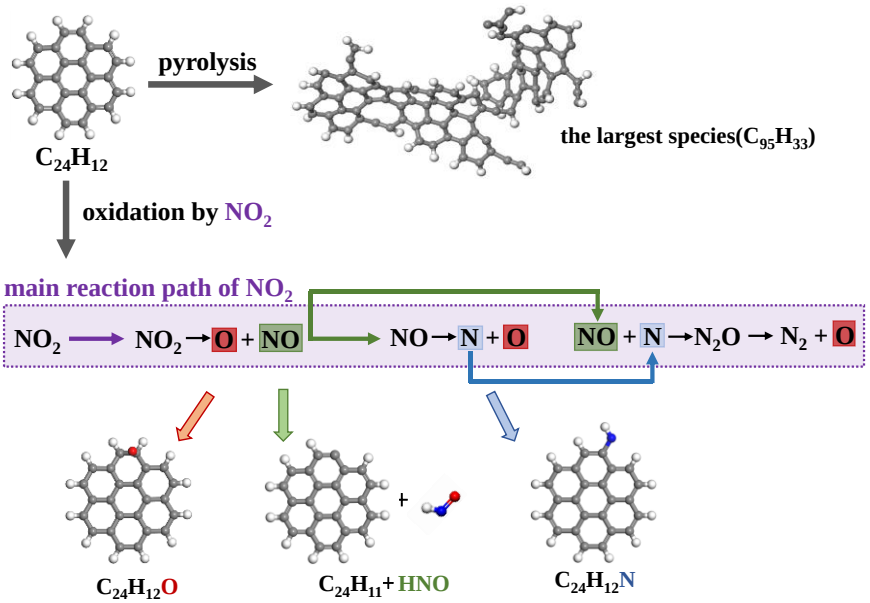

Highlights

- Among the three oxidizers (O_2, NO, and NO_2), NO_2 shows the prominent ability of PAH oxidation, followed by NO and O_2.
- NO_2 decomposes to produce O radicals and NO at 2500 K. NO further decomposes into O and N radicals, which provides resources for PAH oxidation.
- In the systems where $C_{24}H_{12}$ oxidized by NO_X, O radicals play a crucial role in the oxidation of PAH, followed by N radicals.

A ReaxFF molecular dynamics study of polycyclic aromatic hydrocarbon oxidation assisted by nitrogen oxides

Ying Wang[a], Qian Mao[b,c*], Zhanyuan Wang[a], Kai H. Luo[d], Lei Zhou[a,*], Haiqiao Wei[a]

[a] State Key Laboratory of Engines, Tianjin University, Tianjin 300072, China

[b] Institute of Technology for Nanostructures, University Duisburg-Essen, Duisburg 47057, Germany

[c] Institute of Engineering Thermophysics, Chinese Academy of Sciences, Beijing 100190, China

[d] Department of Mechanical Engineering, University College London, Torrington Place, London WC1E 7JE, UK

*Corresponding authors: qian.mao@uni-due.de (Qian Mao); lei.zhou@tju.edu.cn (Lei Zhou)

Abstract

Fossil fuel-derived soot poses a persistent problem. A joint reduction is conducted via the reaction between NO_x and soot. The underlying reaction mechanisms of large polycyclic aromatic hydrocarbons (PAHs), as well as the interactions between O_2, NO and NO_2, have been extensively investigated by ReaxFF molecular dynamics simulations for the first time. The pyrolysis and oxidation of coronene are conducted at 2500 K and 50 atm. Coronene in the pyrolysis system first experiences dehydrogenation reactions and subsequently undergoes recombination reactions, leading to the formation of large PAHs. Among the three oxidizers, NO_2 is the strongest in coronene oxidation, followed by NO and O_2. Meanwhile, the O radical is identified as the key species for PAH oxidation. In the presence of O_2, the formation of O radicals requires the assistance of H radicals that are formed by the dehydrogenation of PAHs, which retards the oxidation process. In the presence of NO, O radicals can be directly formed via reactions of NO → N + O and N + NO ⇌ N_2 + O. NO_2 first undergoes a decomposition reaction: NO_2 → NO + O, followed by NO decomposition. O-addition and N-addition, as well as subsequent fragmentation

reactions including the generation of CO_x and (H)CN are important routes in PAH oxidation. Furthermore, compared to NO, NO_2 provides more O radicals that significantly accelerate PAH oxidation. This study provides fundamental insight into PAH oxidation that may help to design strategies to inhibit soot and NO_x emissions at the source.

Keywords: PAHs; Nitrogen oxides; Oxidation; ReaxFF; Molecular dynamics simulation

1 Introduction

Soot and nitrogen oxides (NO_x) produced from the combustion of fossil fuel cause air pollution as well as human diseases. Increasingly stringent regulations on worldwide emissions have motivated the research and development of clean combustion technologies. In particular, the formation of soot is a complex process consisting of gas-phase reactions [1-3], particle inception [4, 5], coagulation [6, 7], surface reactions (growth [8, 9] and oxidation [10]), and agglomeration [11]. The role of polycyclic aromatic hydrocarbons (PAHs) as the precursors of soot and as its main building block has reached a major consensus within the scientific community [12]. Hydrogen-abstraction-C_2H_2-addition mechanism proposed by Frenklach *et al.* [13] is the most prominent PAH growth pathway. Chu *et al.* [14] found that the percentage of surface hydrogen atoms decreases with the increasing size of PAHs, leading to the preferred reaction pathway changing from H-abstraction to H-addition reactions. As Wang pointed out [15], the aromatic rings must be broken to provide the intermediate species required for PAH growth.

Soot oxidation is a significant and complex process that competes with growth, thus hampering particle emissions. In recent decades, considerable efforts have been devoted to comprehensively understanding the mechanism of PAH oxidation [16, 17]. In an experimental and theoretical study by Dulieu *et al.* [18], the reactivity of O radicals with coronene ($C_{24}H_{12}$) molecules deposited on a graphite surface was elucidated. It was found that oxygenation leads to the fragmentation of $C_{24}H_{12}$. Raj *et al.*

[19] investigated the conversion of 4-pyrenyl to 4-phenanthryl by O_2 using density functional theory (DFT) and developed a detailed reaction mechanism to depict the reactions between O_2 and the free-edge site on soot surfaces. However, O_2 is inefficient for PAH oxidation especially in diesel engines under local fuel-rich combustion conditions, resulting in the massive formation of soot particulates in the exhaust of transportation vehicles. 70% of the 86 million barrels of crude oil in the world are consumed by internal combustion engines (IC). Both NO_x and soot are hazardous pollutants in IC [15]. Experimental studies indicate that soot can be more easily oxidized by NO_2 than O_2 [20, 21]. Most studies focus on the oxidation of soot particles by NO_2 as a post-treatment. Ehrburger *et al.* [22] performed carbon black oxidation experiments in a fixed bed reactor by feeding NO_2 and O_2, and developed a kinetic mechanism of soot oxidation with NO_2 at the exhaust temperature for the first time. Later, Jeguirim *et al.* [23] found that NO_2 molecules are adsorbed mainly on preexisting oxygen complexes, which assists in carbon black oxidation. Tighe *et al.* [24] measured the reaction kinetics of three types of soot by NO_2 and found that soot oxidation is controlled by the intrinsic rate of the surface reaction. Experimental investigations, despite of some efforts in developing techniques to reveal phase and element information [25], have faced some challenges in detailing the chemical mechanisms of PAHs and NO_x. Currently, theoretical studies are limited to small polycyclic aromatic hydrocarbon PAHs and focus on the reactions of a single ring. Li *et al.* [26] conducted the oxidation of a pyrene radical model with a free-edge structure by NO_2 using the DFT method. This study confirmed the reaction pathway of soot oxidation with NO_2 proposed by Ehrburger [22]. In addition, there have been a few studies on the influence of nitrogen oxides on the formation and oxidation of soot precursors during the combustion process. In the study of Abián *et al.* [27], pyrolysis experiments of ethylene in the presence of different NO_x (NO, NO_2 and N_2O) were carried out at atmospheric pressure, in the temperature range of 975–1475 K. It was reported that the

lowest soot tendency was achieved in the presence of NO_2, followed by NO and N_2O. Diesel engines are widely used by virtue of their favorable power performance, which causes serious environmental pollution. The oxidation of soot by NO_x inevitably occurs in the soot oxidation zone [28] at the flame surface in the spray flame. Note that more than 90% of the soot formed in diesel engines is eliminated in the combustion before the exhaust gases leave the cylinder [29, 30]. Therefore, uncovering the underlying mechanism and detailed reaction pathways of PAH oxidation assisted by O_2 and NO_x at high temperature and pressure conditions is of significant interest.

To reveal the underlying oxidation mechanism of PAHs, it is necessary to perform a fundamental theoretical study at the atomistic scale. The computational expense makes quantum chemistry methods inapplicable for large PAH species and large systems. Moreover, classical molecular dynamics (MD) allows for large-scale simulations but is not appropriate to describe chemical reactions. ReaxFF MD is suitable for exploring the complex processes of bond breaking and forming without any pre-defining pathways, and it offers the possibility of simulating the reactive PAH systems [31-34] at large lengths and time scales.

In this paper, the ReaxFF MD method was utilized to investigate the reaction mechanisms of large PAH pyrolysis and oxidation at high temperature and pressure conditions for the first time. The present study emphasizes the detailed reaction pathways of large PAH oxidation by NO and NO_2 from an atomistic perspective. Meanwhile, novel insights into the key reactive events related to PAH pyrolysis and oxidation are obtained, which potentially helps to develop comprehensive kinetic mechanisms and soot reduction strategies.

2 Methodology

2.1 Simulation method

ReaxFF molecular dynamics (MD) was developed to bridge the gap between quantum mechanics and classical force field methods, while largely retaining the accuracy of quantum mechanics and the computational efficiency of the classical MD [35, 36]. The ReaxFF force field is a force field based on the bond order, which was first introduced by Tersoff *et al.* [37] in the development of a force field for silicon and was extended to a carbon system by Brenner *et al.* [38]. The ReaxFF force field includes the following energy components:

$$E_{syst} = E_{bond} + E_{over} + E_{under} + E_{lp} + E_{val} + E_{tor} + E_{vdWaals} + E_{Coulomb} \quad \text{(Eq. 1)}$$

where terms on the right-hand side of the equation represent bond energy, over-coordination energy penalty, under-coordination stability, lone pair energy, valence angle energy, torsion angle energy, van der Waals energy, and Coulomb energy, respectively [39, 40]. A more detailed description of the ReaxFF force field can be found in the work by van Duin *et al.* [41, 42].

2.2 Verification of the ReaxFF force field

ReaxFF for the oxidation of hydrocarbons was first developed by van Duin *et al.* [41] and then improved by Chenoweth *et al.* [43] in 2008 (CHO-2008). However, the CHO-2008 force field can only predict the combustion chemistry of larger hydrocarbons (> C3). Ashraf and van Duin reparametrized the ReaxFF force field (CHO-2016) [44] based on CHO-2008 to ensure its transferability to the oxidation and pyrolysis of hydrocarbon fuel, irrespective of molecular size or structure. Later, Kowalik *et al.* [45] extended CHO-2016 to the C/H/O/N system (CHON-2019). The bond/angle/dihedral parameters that involve N are trained against available experimental and DFT data. Another set of C/H/O/N ReaxFF force field (CHONS-2012) was utilized by Li *et al.* [46] to describe the coal pyrolysis and oxidation process. Therefore, validations of both the CHON-2019 and CHONS-2012 force fields are performed via simulating the pyrolysis and oxidation of cyclopentadiene(C_5H_6) and benzene (C_6H_6) at 2500 K and

50 atm, as shown in Fig.1(a) and (b), respectively. Note that C_5H_6 and C_6H_6 are typically regarded as the first aromatic ring in PAH formation. The oxidations take place in the presence of different oxidizers (O_2, NO, NO_2). The dissociation energies for the cleavage of the C−H bond of C_6H_6 and C_5H_6 are 110.8 kcal/mol [47] and 84.8 kcal/mol [48], respectively. Therefore, C_5H_6 should react more easily than C_6H_6. However, it can be seen in the red box in Fig. 1(b) that C_6H_6 is consumed at a faster rate than C_5H_6 in the presence of NO_2 with the CHONS-2012 force field. In addition, experimental results show that NO_2 is a more efficient oxidizer compared with NO [27]. Nonetheless, C_5H_6 decreases faster in the latter stage in the presence of NO, as shown in the blue block. Overall, the CHON-2019 force field is more suitable for the simulation of systems in which hydrocarbons are oxidized by NO_x.

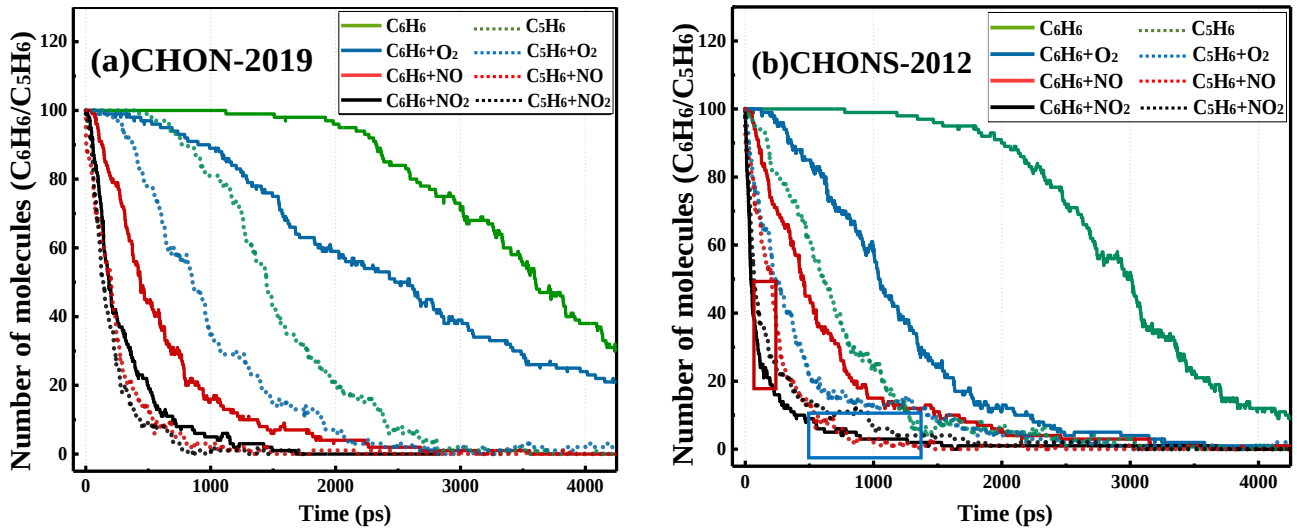

Fig. 1. Time evolution of the C_6H_6/C_5H_6 molecule number for systems with different oxidizers utilizing (a) CHON-2019 and (b) CHONS-2012.

We further validate the ReaxFF force field of CHON-2019 by comparing the bond dissociation energies (BDEs) of NO_x against quantum chemistry calculations [49] as the decomposition of NO_x are initiation reactions for the NO_x and PAH system at high temperatures. The CBS-QB3 method is validated to be accurately predicted the BDEs of NOx species [49]. Table 1 shows the calculated BDEs of NO_2

and NO from the CBS-QB3, and the CHON-2019 force field, respectively. The CBS-QB3 method gives a NO_2 BDE of 74.2 kcal/mol. The BDE of NO_2 predicted by the CHON-2019 force field is almost the same as that from the CBS-QB3 method by a difference of just 0.77 kcal/mol. NO is a diatomic molecule with a BDE of 151.68 kcal/mol from the CBS-QB3. The BDE from the CHON-2019 force field is relatively higher than that from CBS-QB3 by a difference of 8.91 kcal/mol. The relative error of the ReaxFF CHON-2019 force field in describing the BDE energies of NO_x is around 5%, which is acceptable for MD simulations [43]. Results from above indicate that the CHON-2019 force field can accurately predict the decomposition of NO_x.

Table 1. Bond dissociation energies of NO_2 and NO with quantum chemistry methods and the ReaxFF Force Field (Unit: kcal/mol)

	CBS-QB3	ReaxFF	ReaxFF deviation from CBS-QB3	
			absolute difference	relative difference (%)
NO_2	74.20	73.43	0.77	1.03
NO	151.68	160.65	8.91	5.87

2.3 Computational details

The ReaxFF MD simulation is carried out with the REAXC package in the Large-scale Atomic/Molecular Massively Parallel Simulation (LAMMPS) [50]. Coronene, with a highly symmetric stable structure, is a common type of PAH formed during the incomplete combustion of hydrocarbon fuels. Meanwhile, it has attracted attention as it is proposed to be the precursor for nascent soot inception [51-53]. In accordance with the force field validation in Section 2.2, the CHON-2019 ReaxFF force field [45] was used for MD simulations in the current work. The setups of the ReaxFF MD simulations are shown in Table 2, including pyrolysis and oxidation by O_2, NO and NO_2. The system in which O_2 is used as an oxidizer contains 100 $C_{24}H_{12}$ and 1350 O_2 molecules corresponding to an equivalence ratio of 2. To investigate the effect of nitrogen oxides on $C_{24}H_{12}$ oxidation, O_2 is replaced by NO and NO_2 with the same molecule number. To maintain the same initial mole fraction of $C_{24}H_{12}$ in different systems, Ar

acts as the bath gas is added, and the interaction between Ar and other species occurs via the van der Waals interactions [54]. Periodic boundary conditions are implemented in three directions. The bond order cutoff for molecular recognition is set to 0.2 in gas-phase systems [55]. Energy minimization is applied before simulations via the conjugate gradient algorithm to eliminate artificial effects. MD simulations are performed with the isothermal–isobaric ensemble (NPT) with constant atom number, pressure, and temperature. The pressure is set to 50 atm, which is of practical importance for high-pressure combustion engines and suitable for the ReaxFF MD simulation timescale [56]. The system temperature is maintained by the Nosé-Hoover thermostat with a damping constant of 50 fs. A Nose-Hoover barostat was used to relax the pressure with a damping constant of 100 fs. The starting configurations are equilibrated for 200 ps with a time step of 0.1 fs at 300 K. Then, the MD simulations are carried out for 4000 ps with a time step of 0.2 fs at 2500 K [56]. Three replicas with unique starting configurations were conducted for each simulation case.

Table 2 Simulation conditions of $C_{24}H_{12}$ pyrolysis and oxidation.

System	Molecules	Temperature (K)	Pressure (atm)
$C_{24}H_{12}$	$100C_{24}H_{12}$+2700Ar	2500	50
$C_{24}H_{12}+O_2$	$100C_{24}H_{12}+1350O_2+1350$Ar		
$C_{24}H_{12}$+NO	$100C_{24}H_{12}$+1350NO+1350Ar		
$C_{24}H_{12}+NO_2$	$100C_{24}H_{12}+1350NO_2+1350$Ar		

3 Results and Discussion

First, a global analysis of the pyrolysis and oxidation of $C_{24}H_{12}$ is conducted. It is difficult for $C_{24}H_{12}$ to react at temperatures lower than 2000 K under both pyrolysis and oxidation by O_2 conditions. Fig. 2 shows the time evolution of the number of $C_{24}H_{12}$ molecules under pyrolysis and oxidation conditions with different oxidizers (O_2, NO, NO_2) at 2500 K. Compared to NO and NO_2, O_2 is the weakest oxide for $C_{24}H_{12}$, and NO_2 shows the best oxidation ability for $C_{24}H_{12}$, which is in good agreement with

experiments [27]. Fig. 3 shows the proportion of different reaction types that trigger the first-step reaction of $C_{24}H_{12}$. The reaction pathway and the reaction type are identified by the Chemical Trajectory Analyzer (ChemTraYzer) [57], which extracts trajectory information. In the pyrolysis system, the H-addition reaction accounts for the largest proportion (29.8%). 17.5% of $C_{24}H_{12}$ experience H-abstraction by H radicals. However, in the simulation on benzene pyrolysis under the same condition, 22.0 % and 20.7% of benzene experienced H-abstraction by H and H-addition as the initial step, respectively. The percentage of surface hydrogen atoms decreases with PAH size, leading to a change in the preferred reaction pathway from H-abstraction by H to H-addition reactions [14]. The proportion of C_xH_y species addition was found to be 21.9%, as shown by the light blue column in Fig. 3. Reactions during pyrolysis (including dehydrogenation, H-addition, H-abstraction by H radicals and C_xH_y species addition) occur actively in the $C_{24}H_{12}$+O_2 system. However, the proportion of H-abstraction by H and H-addition decreased compared with the pyrolysis system since a large number of H radicals generated by dehydrogenation are involved in the reaction with oxygen. In the system where $C_{24}H_{12}$ is oxidized by NO_x, the first-step reactions differ considerably from the above system. In the presence of NO and NO_2, most $C_{24}H_{12}$ molecules are initiated by the reaction with O radicals or N radicals, shown in blue and green, respectively. The reactions with O/N consist of two types, O/N-addition and H-abstraction by O/N. Among them, the O/N-addition reaction plays a more important role, which can be attributed to the large C/H ratio. The most common structures of $C_{24}H_{12}O$ and $C_{24}H_{12}N$ in simulations are shown in Fig. 3. The detailed reaction pathways under different conditions are discussed separately in the following sections.

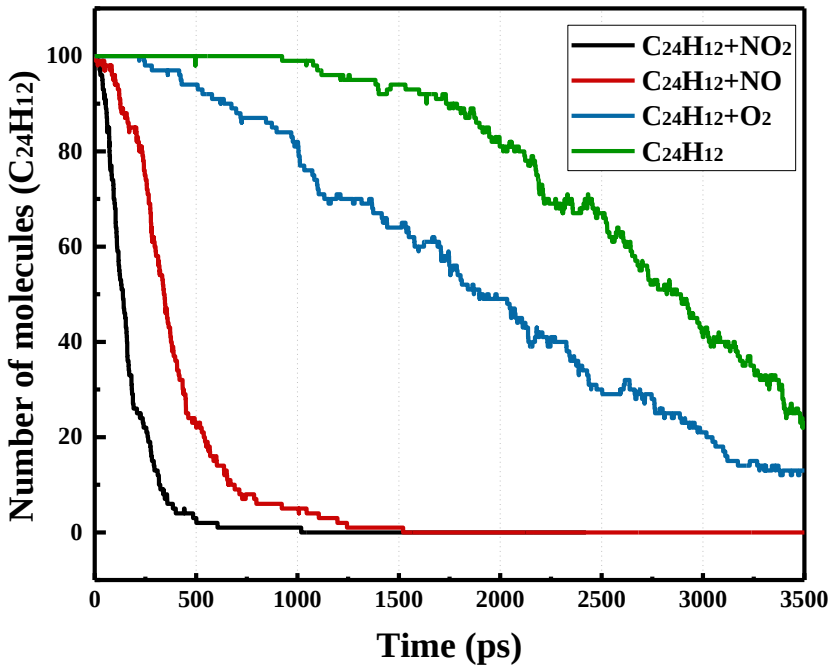

Fig. 2. Time evolution of the $C_{24}H_{12}$ molecule number in systems under pyrolysis and oxidation conditions with different oxidizers (O_2, NO, NO_2) at 2500 K.

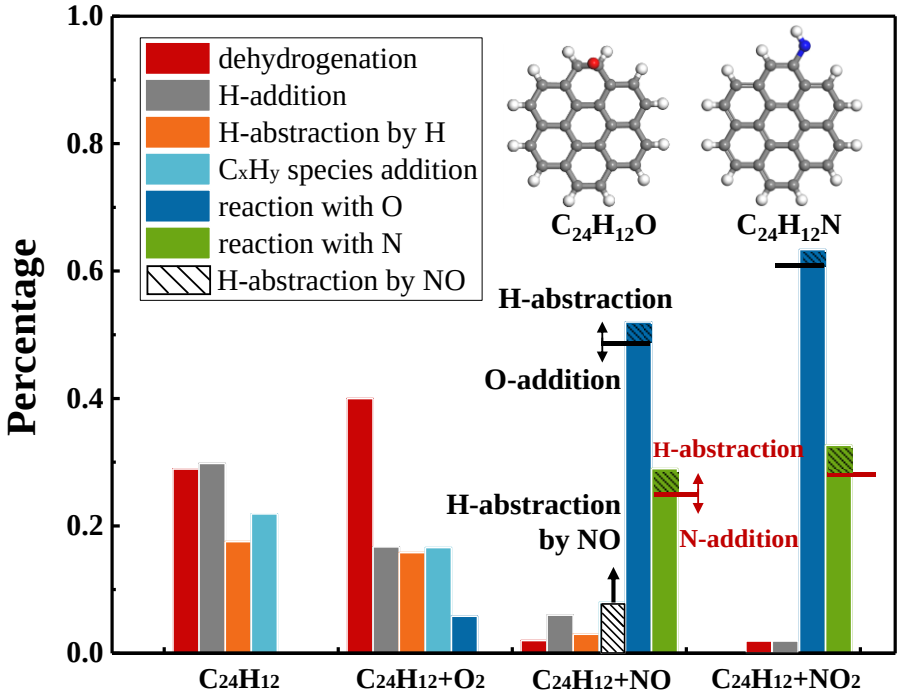

Fig. 3. Proportion of the main first-step reactions of $C_{24}H_{12}$ in systems under pyrolysis and oxidation conditions with different oxidizers (O_2, NO, NO_2) at 2500 K.

3.1 Pyrolysis of coronene

The pyrolysis of $C_{24}H_{12}$ at high temperatures was studied. The time evolution of the number of species with different carbon numbers is counted during $C_{24}H_{12}$ pyrolysis at 2500 K as shown in Fig. 4. The decomposition of $C_{24}H_{12}$ starts at 924.0 ps when the molecule number starts to decrease. Based on the MD trajectory, the dehydrogenation reaction mainly occurs from 924.0 ps to 1628.4 ps, accompanied by a small amount of H-addition and H-abstraction reactions. Note that the dehydrogenation process destroys the stable structure of $C_{24}H_{12}$ and triggers further dehydrogenation or C-C bond breaking. According to the proportion of the first-step reaction shown in Fig. 3, 28.9% of $C_{24}H_{12}$ is initiated by dehydrogenation under the pyrolysis condition. H radicals formed from dehydrogenation then contribute to the H-addition (29.8%) and H-abstraction (17.5%) of $C_{24}H_{12}$. After 1628.4 ps, the cleavage of the C-C bond in PAH radicals produces small species. This consequently leads to an increase in $C_{1\text{-}9}$ species. As shown in Fig. 4(a), species with two carbon atoms, including C_2, C_2H, and C_2H_2, are the most dominant products of decomposition. Meanwhile, PAH growth occurs during PAH pyrolysis. The formation of large PAHs is the key step in bridging the gap between gaseous fuel molecules and solid soot particles [15]. An elevated C/H ratio [58] and an increase in the number of C_xH_y [59] promote the growth of PAH. A species with 48 carbon atoms emerges at 1997.0 ps. After that, as seen in Figs. 4(d), (e) and (f), large species are formed in the late stage. Specifically, the largest species ($C_{95}H_{33}$) is captured at 3985.8 ps in the system, which is large enough to be termed a nascent soot particle [60] with a 3-dimensional structure. The C/H ratio of $C_{95}H_{33}$ is much higher than that of $C_{24}H_{12}$, indicating that the formation of the nascent soot particle is also accompanied by graphitization, which is consistent with the statistical results of PAH growth [61, 62].

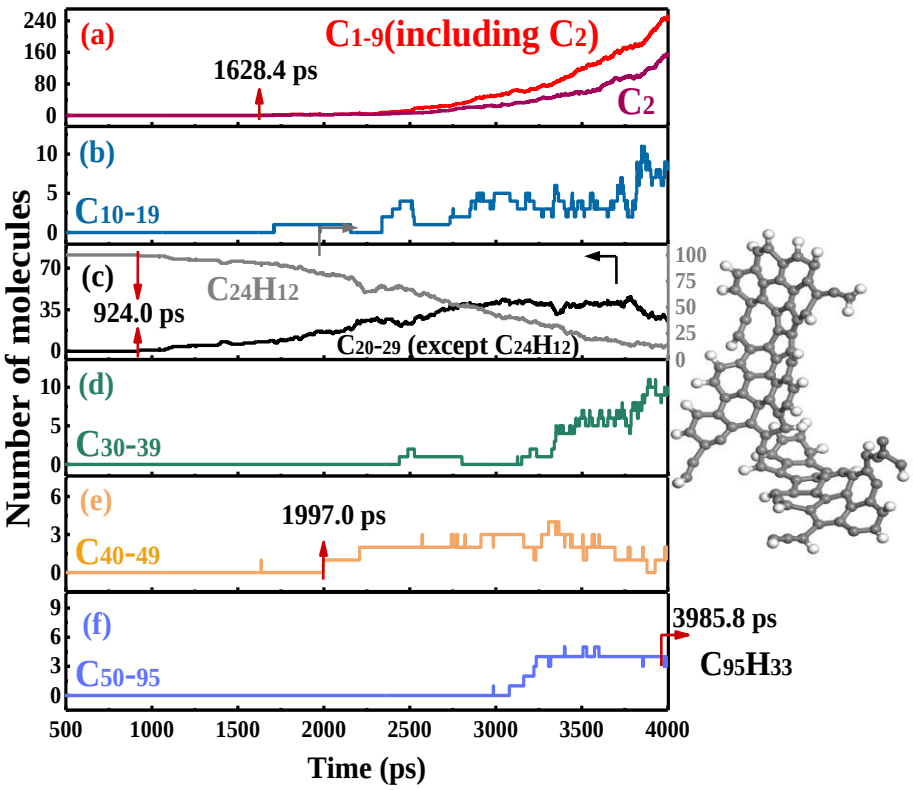

Fig. 4. Time evolution of the number of molecules with different carbon numbers in the $C_{24}H_{12}$ pyrolysis system.

3.2 Oxidation of coronene

3.2.1 Effect of O_2

Oxygen is one of the most common oxidizers in the combustion process. As shown in Fig. 5, the presence of oxygen molecules prompts the reaction to start earlier than the pyrolysis of $C_{24}H_{12}$. The number of larger hydrocarbons (>C50) is less than that in the $C_{24}H_{12}$ pyrolysis system and $C_{75}H_{33}O_2$ is observed as the largest species in the $C_{24}H_{12}$+O_2 system.

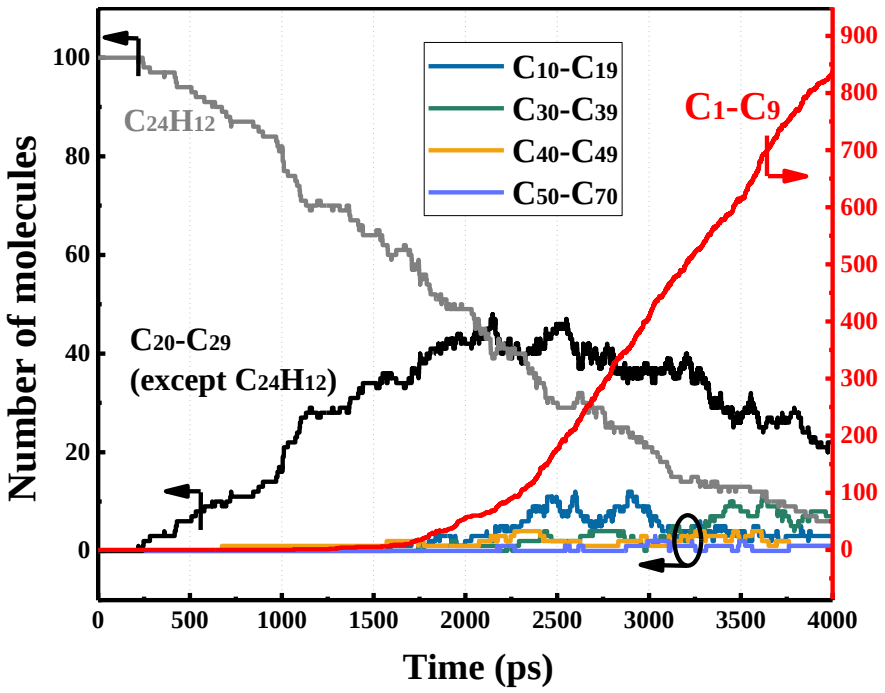

Fig. 5. Time evolution of the number of molecules with different carbon numbers in the $C_{24}H_{12}$+O_2 system.

Fig. 6 shows the main reaction pathways and the number of reactions in the $C_{24}H_{12}$+O_2 system at 2500 K within the first 4000 ps. Similar to the pyrolysis conditions, in the presence of O_2, the reaction of $C_{24}H_{12}$ still starts with dehydrogenation, which provides H radicals for subsequent reactions. Meanwhile, reactions including H-addition and H-abstraction by H radicals still account for a significant proportion of the $C_{24}H_{12}$ consumption, with percentages of 16.7% and 15.8%, respectively (Fig. 3). Minimal O_2 molecules are directly involved in the oxidation, only two H-abstraction by O_2 were observed. Most O_2 molecules react with H radicals via R1, which is a chain-branching reaction producing O and OH radicals,

$$O_2 + H \rightarrow O + OH \quad \text{(R1)}$$

A large number of H radicals are consumed by R1. As a result, the percentage of dehydrogenation of $C_{24}H_{12}$ is much higher than that in the pyrolysis system to supply more H radicals, as shown in Fig. 3. In

addition, R1 is also the most important reaction producing O radicals. The reaction of the O radical and $C_{24}H_{12}$ initially proceeds via O-addition to C atoms, producing oxygenated species. The energetically preferable locus for oxide attack is the free-edge site [63]. As shown in Fig. 6, the species with an O radical attached to a C atom in the outer edge position (a) or between two C atoms in the outer edge position (b) are most frequently observed. In the DFT study by Dulieu [18], the O-addition reactions forming species (a) and (b) are exothermic at energies of -21.45 kcal/mol and -16.37 kcal/mol, respectively, and the energy barriers of the corresponding transition states are 2.54 kcal/mol and 23.75 kcal/mol, respectively, indicating that structure (a) is preferred. In the oxidation systems including $C_{24}H_{12}$+O_2, $C_{24}H_{12}$+NO and $C_{24}H_{12}$+NO_2, more than 90% of the O-addition reactions lead to the formation of species (a). A more detailed analysis of the reaction with NO and NO_2 will be presented in Section 3.2.2. In the $C_{24}H_{12}$+O_2 system, the number of O radicals is limited by insufficient H radicals at the beginning. Therefore, only approximately 5% of $C_{24}H_{12}$ molecules react with O radicals. Afterward, the O radicals effectively participate in the subsequent oxidation reactions of $C_{24}H_{12}$. Most O radicals undergo an addition reaction to the C atoms and eventually form carbon oxides. A small portion of O radicals takes the H-abstraction reactions of PAHs. Similarly, the reaction with OH is dominated by OH-addition (154 times), while H-abstraction by OH (13 times) is a minor contributor. The dominance of addition reactions is attributed to high temperatures as well as large molecular sizes [64].

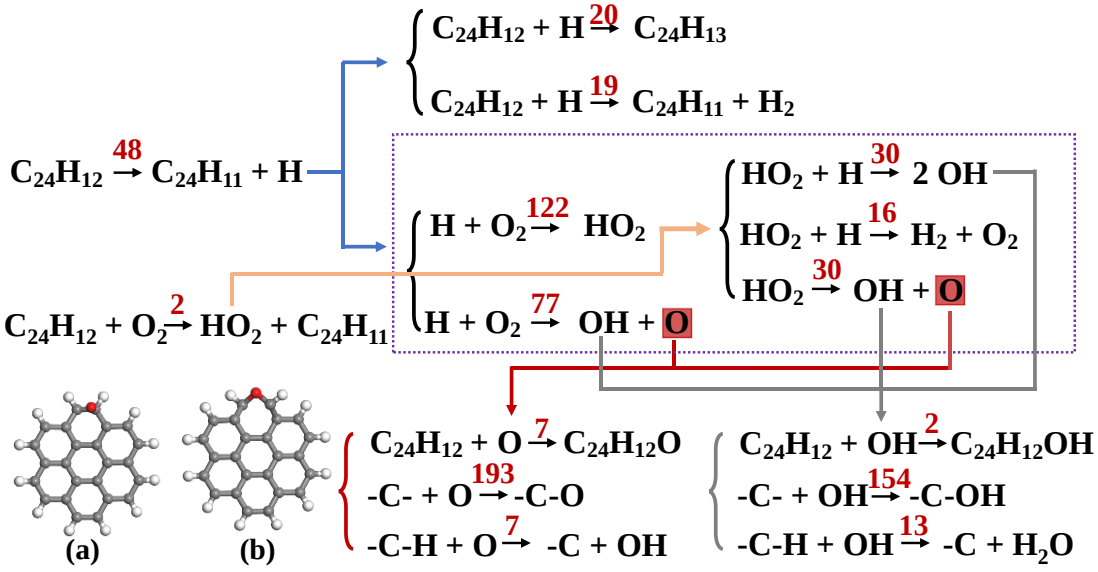

Fig. 6. Reaction pathways of $C_{24}H_{12}$ oxidation by O_2. The number of reactions is indicated in red.

3.2.2 Effect of NO_x

NO_x has been proven to significantly contribute to soot reduction [65]. With the same simulation time and initial conditions, the number of large hydrocarbons (>C30) is significantly less than that in the pyrolysis system and oxidation system with O_2, as seen in Fig. 7. The $C_{24}H_{12}$+NO_2 system has the smallest number of large species, followed by $C_{24}H_{12}$+NO and $C_{24}H_{12}$+O_2. In addition, $C_{47}H_{24}O$ and $C_{33}H_{11}N_6O_2$ are observed as the largest species in the $C_{24}H_{12}$+NO and $C_{24}H_{12}$+NO_2 systems, respectively. Overall, NO_2 shows a prominent ability to inhibit soot formation. However, the underlying mechanisms of NO and NO_2 on soot oxidation are still not clear, especially under high temperature and pressure conditions.

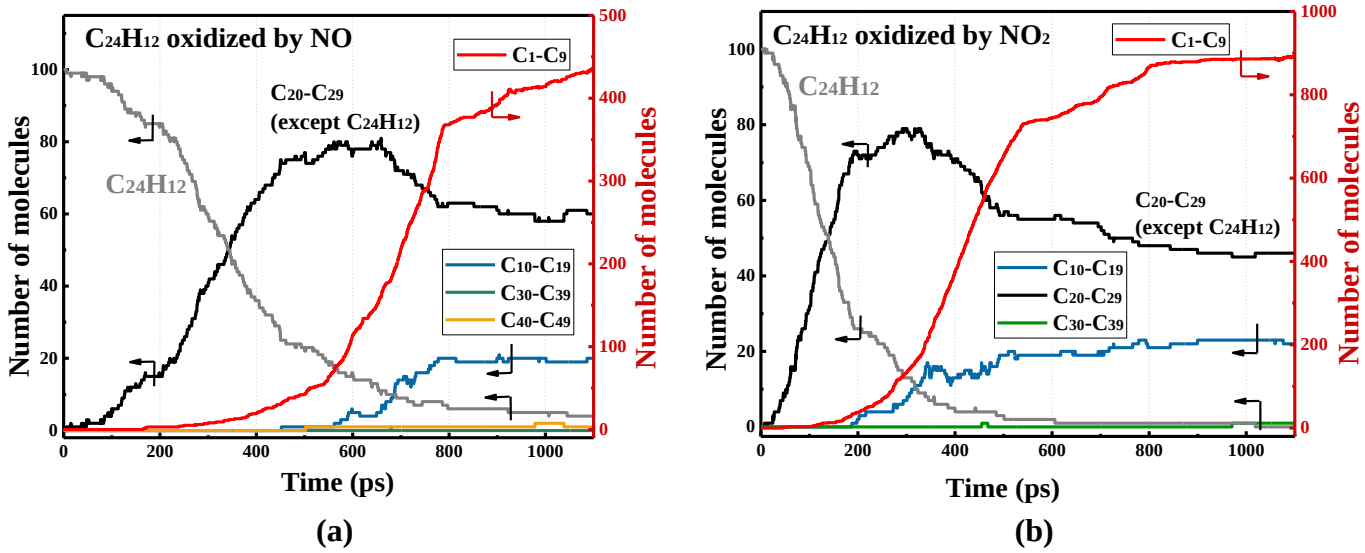

Fig. 7. Time evolution of the number of molecules with different carbon numbers in the systems of (a) $C_{24}H_{12}$+NO, and (b) $C_{24}H_{12}$+NO_2.

3.2.2.1 Effect of NO

According to the evolution of the species shown in Fig. 3, in the presence of NO or NO_2, the number of $C_{24}H_{12}$ is close to zero at 1200 ps. Therefore, we focus on the oxidation process before 1200 ps. Fig. 8 shows the reaction pathways before 1200 ps, where the numbers of different reactions in the system of $C_{24}H_{12}$ oxidation by NO are represented in red. Note that, the blue numbers indicate the number of reactions in the NO system where the reaction of NO is conducted independently, with simulations performed at 2500 K and 50 atm. The dashed arrows and the green dashed block indicate that the reaction pathways only occur in the pure NO system. The reactions in the red dashed block take place in the $C_{24}H_{12}$+NO system. -C-H or -C-C represents the active site for the reaction of the carbon-containing molecules in the oxidation process. There are two main reaction routes of NO. Firstly, in the $C_{24}H_{12}$+NO system, NO is effective for H-abstraction, which agrees well with the study by Xu *et al.* [66]. 8% of $C_{24}H_{12}$ molecules are triggered by the H-abstraction with NO. Secondly, for both the $C_{24}H_{12}$+NO system and pure NO systems, the reaction pathways of NO decomposition are as follows:

$$NO \rightarrow N + O \quad \text{(R2)}$$

$$N + NO \rightarrow N_2 + O \quad \text{(R3)}$$

$$N + NO \rightarrow N_2O \quad \text{(R4)}$$

$$N_2O \rightleftharpoons N_2 + O \quad \text{(R5)}$$

The production of N_2 in R3 is consistent with the results observed in the experiment [67]. NO decomposes into O and N radicals, providing reactive species for PAH oxidation. Meanwhile, N radicals further react with NO. On the one hand, NO reacts with N by forming N_2 and O radicals (R3). On the other hand, N_2O is generated by the addition reaction (R4), which can further decompose to N_2 and O (R5). The reaction of R5 is forward-driving as it happens 167 times without the reverse reaction in the system of $C_{24}H_{12}$ oxidation by NO. In the magnified image of N_2O in Fig. 9, the number of N_2O is quite marginal and fluctuates a lot in the system of $C_{24}H_{12}$ oxidation by NO, indicating that N_2O is not important in $C_{24}H_{12}$ oxidation. In contrast, the reverse reaction of R5 is counted as 420 times in the pure NO system. At this point, N_2O can further react with N and O radicals and subsequently produce N_2 and NO as shown in the green dashed block in Fig. 8. This phenomenon can be explained by the consumption routes of O radicals. In the pure NO system, the concentration of O radicals increases dramatically via R2 and R3, providing opportunities to collide with N_2. Therefore, the reverse reaction of R5 takes place. In addition, abundant O radicals react with N_2O by producing NO:

$$N_2O + O \rightarrow 2NO \quad \text{(R6)}$$

which produces a large amount of NO, and the reaction loop is repeated as indicated by the green dashed line. Eventually, equilibrium is reached in the pure NO system. However, in the system where $C_{24}H_{12}$ is oxidized by NO, O radicals are actively involved in $C_{24}H_{12}$ oxidation, as indicated by the solid red arrow. Since O radicals are not sufficiently produced in the system, R5 is forward-oriented to provide more O radicals for hydrocarbon oxidation. As shown by the blue arrow, a large proportion of N radicals produced by the cleavage of NO participate in R3 and R4 in both systems. Similar to the fate of O

radicals, in the pure NO system, N radicals participate in the reaction with N_2O and generate NO, which re-enters into the cycle:

$$N_2O + N \rightarrow N_2 + NO \quad (R7)$$

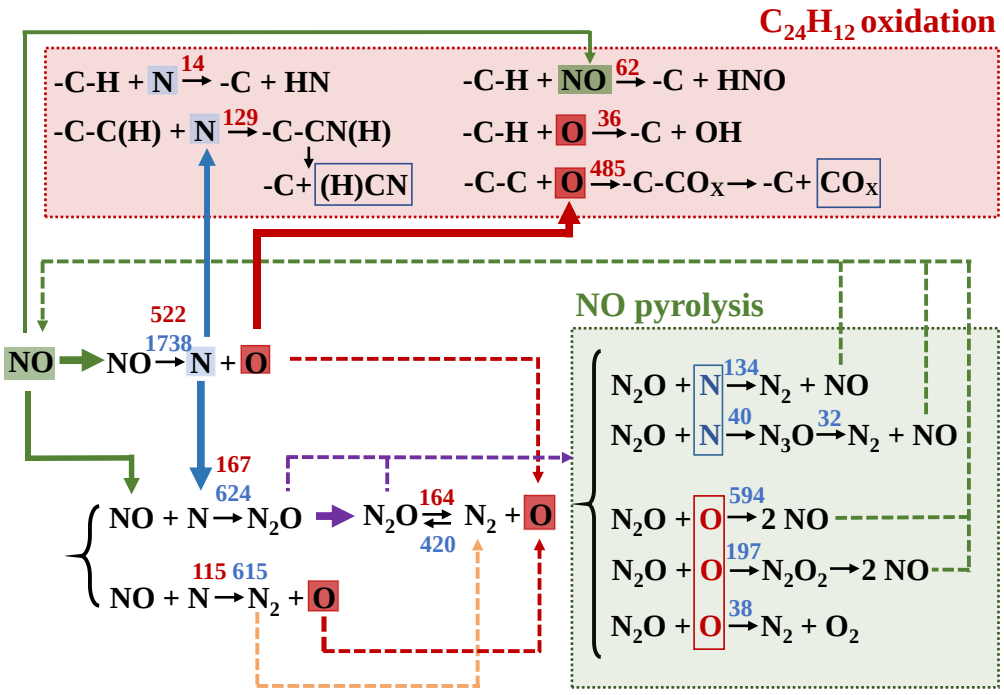

Fig. 8. Reaction pathways of the NO system and the $C_{24}H_{12}$+NO system. The numbers of reactions in the NO system and the $C_{24}H_{12}$+NO system are indicated in blue and red, respectively. The dashed lines indicate the processes that are only discovered in the pure NO system.

However, in the $C_{24}H_{12}$+NO system, N radicals are involved in the oxidation of $C_{24}H_{12}$. Fig. 9 shows the time evolution of species for the system of $C_{24}H_{12}$ oxidation by NO at 2500 K. The arrows on the left side indicate the values of O, N_2, NO, and N at 1200 ps in the pure NO system. The amounts of O, N, and N_2 are lower in the oxidation system than in the pure NO system. In particular, the reduction of O radicals is the most pronounced, with a difference of 700. The slowdown in NO consumption can be attributed to the weakening of R3 and R4, as the consumption of PAHs competes for N radicals. It can be concluded that both N and O are significantly involved in the oxidation of $C_{24}H_{12}$. The reactions of

H-abstraction by O and O-addition are found in the first step of $C_{24}H_{12}$, as shown in Fig. 3. However, H-abstraction by O radicals accounts for only 3%, which is much lower than the O-addition reaction (49%). This results from the higher energy barrier of 17.07 kcal/mol for the H-abstraction reaction compared to 2.54 kcal/mol for the O-addition reaction [18]. The reaction pathways of O-addition and fragmentation with CO and CO_2 are progressively released. At 1200 ps, 311 CO and 10 CO_2 are detected in the system. CO_x has an inhibitory effect on soot formation, as it ties up carbon atoms, limiting their involvement in soot formation processes. Meanwhile, N radicals also contribute to the fragmentation of $C_{24}H_{12}$. Depending on whether or not the H atom is attached to carbon, it is eventually fragmented into HCN/HNC or CN.

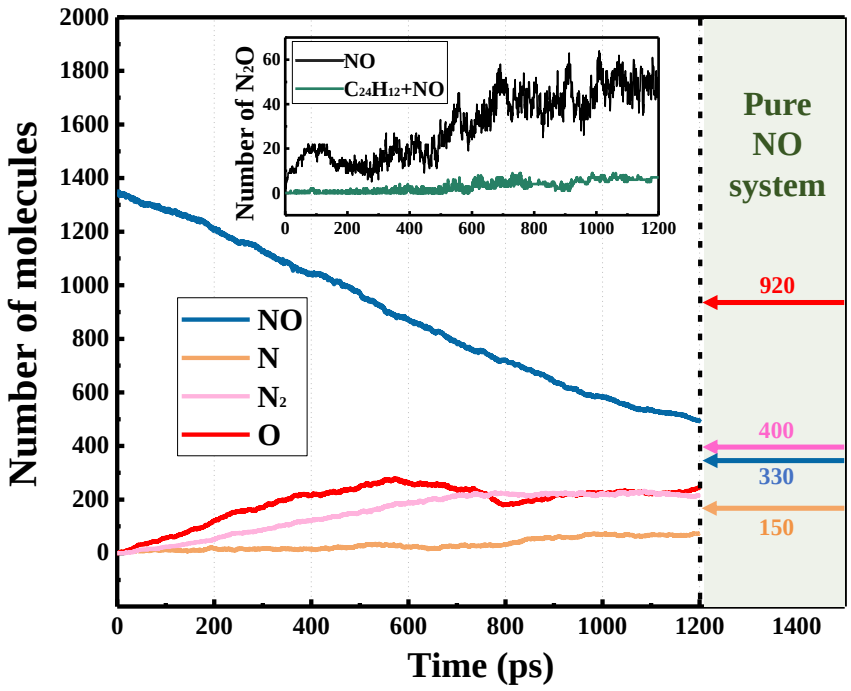

Fig. 9. Time evolution of the molecular numbers of NO, N_2, N, and O in the $C_{24}H_{12}$+NO system before 1200 ps. The arrows on the right side show the number of NO, N_2, N, and O at 1200 ps in the pure NO system.

3.2.2.2 Effect of NO_2

In the present work, NO_2 demonstrated a superior ability to eliminate $C_{24}H_{12}$. Fig. 10 shows the reaction pathways of the pure NO_2 system and the system of $C_{24}H_{12}$ oxidation by NO_2 at 2500 K. The main reaction route of NO_2 acts as a rich source of O and N radicals for both systems via:

$$NO_2 \rightarrow NO + O \quad \text{(R8)}$$

$$NO \rightarrow N + O \quad \text{(R2)}$$

In addition to the main reaction pathway, the remaining NO_2 reacts with O and N radicals, and eventually generates NO, as shown by the purple arrows. In the presence of $C_{24}H_{12}$, with the presence of H radicals from dehydrogenation, some NO_2 molecules are converted to NO through:

$$NO_2 + H \rightarrow NO + OH \quad \text{(R9)}$$

Most OH radicals react with O and N radicals to reproduce H radicals. Compared to the effect of NO, the increase in the number of O radicals is the most intuitive difference in the NO_2 system.

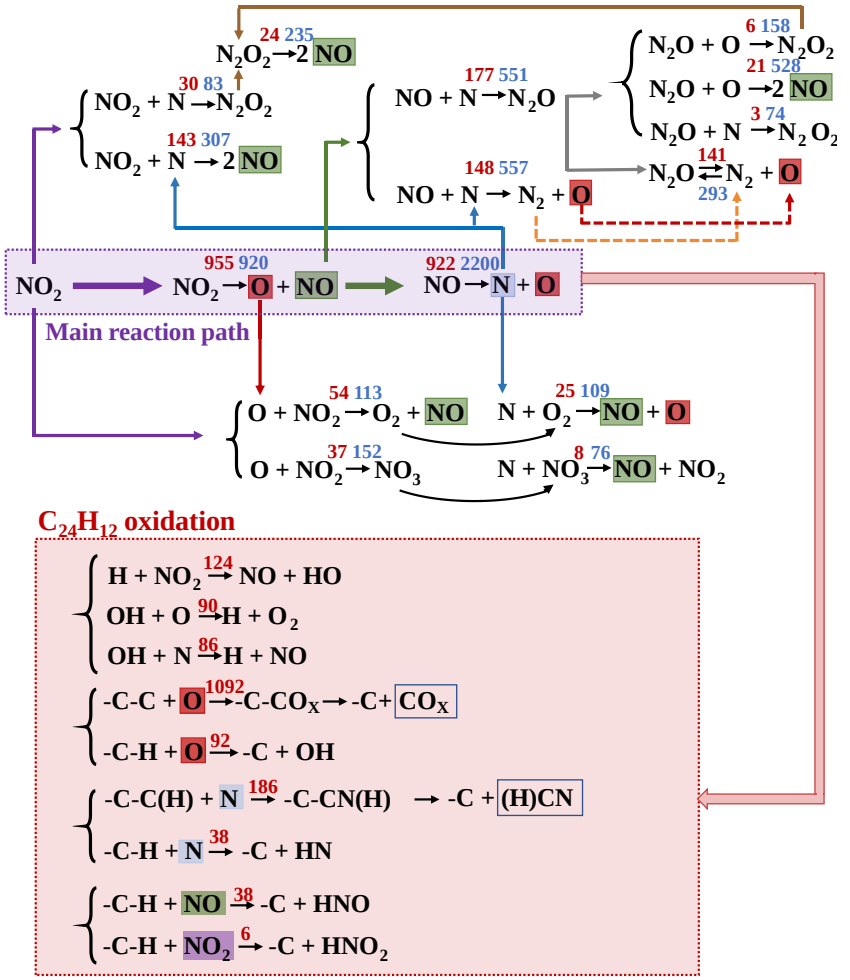

Fig. 10. Reaction pathways of the pure NO_2 system and the $C_{24}H_{12}$+NO_2 system. The numbers of reactions in the NO_2 system and the $C_{24}H_{12}$+NO_2 system are indicated in blue and red, respectively. Dashed lines indicate that the processes are only discovered in the pure NO_2 system.

Fig. 11 shows that approximately 800 O radicals are generated in the $C_{24}H_{12}$ oxidation system by NO_2 in 1200 ps, which is 1400 less than in the pure NO_2 system. Most O radicals are involved in the oxidation of PAHs and produce CO or CO_2. As a result, 737 CO and 32 CO_2 are generated. The presence of a large number of O radicals also triggers the progression of R6, which has not been observed in the oxidation of $C_{24}H_{12}$ by NO. Furthermore, the increase in O radicals promotes the role of N radicals in the oxidation process. More N radicals participate in the reactions of N-addition and H-abstraction of hydrocarbons compared to the $C_{24}H_{12}$+NO system. It can be seen from Fig. 7(b), in the presence of NO_2,

the degree of fragmentation is enhanced, which is manifested by the increase in the total molecule numbers. Therefore, N radicals generated by R2 have more opportunities to participate in PAH oxidation. Overall, the role of NO_x is mainly to modify the composition and quantity of the radical pool, especially in the generation of O and N radicals.

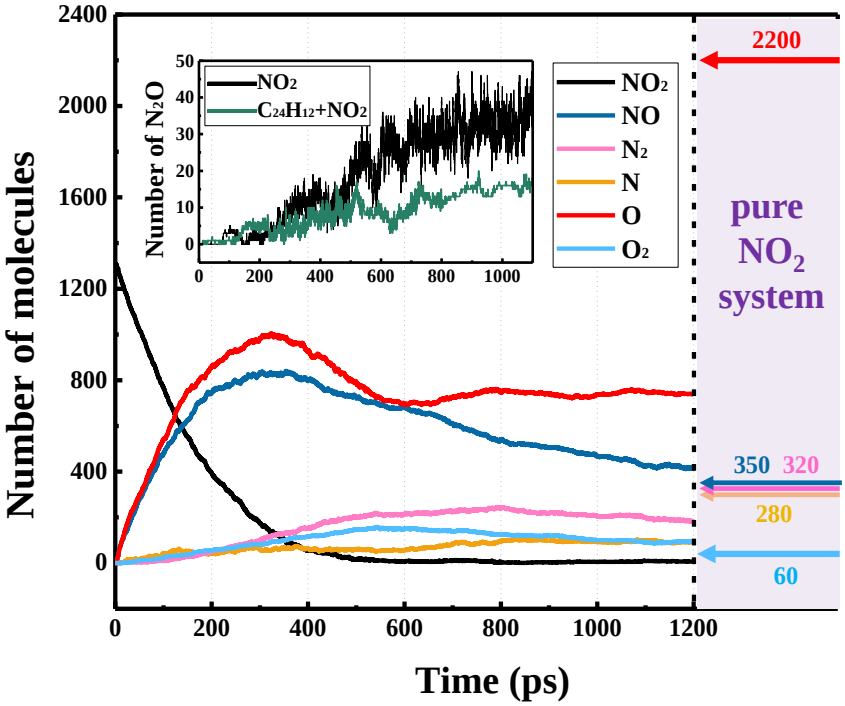

Fig. 11. Time evolution of the molecule number of NO_2, NO, N_2, O_2, N, and O in the $C_{24}H_{12}+NO_2$ system before 1200 ps. The arrows on the left side show the number of NO_2, NO, N_2, O_2, N, and O at 1200 ps in the pure NO_2 system.

Furthermore, the oxidation of coronene and the opening of the first aromatic ring in the oxidation system were investigated. Fig. 12 shows the oxidation pathway of $C_{24}H_{12}$ under attack from O and N radicals. Starting from the O-addition at site (a), the migration of the H radical from site (a) to the adjacent C is observed. Subsequently, an N radical is added to an adjacent ring. After the cleavage of the C-C bond, the first ring opens and leads to species (5). Later, the C-H bond connects to another C in the ring, and the C=O bond is exposed at the edge after the cleavage of the C-C bond (species 5-6-7). From species

(5) to (6), the H attached to the C transfers to the adjacent N with a low barrier [68]. Finally, the CO and HNC located at the edge are removed, which leads to the cleavage of the first ring, as seen in species (9).

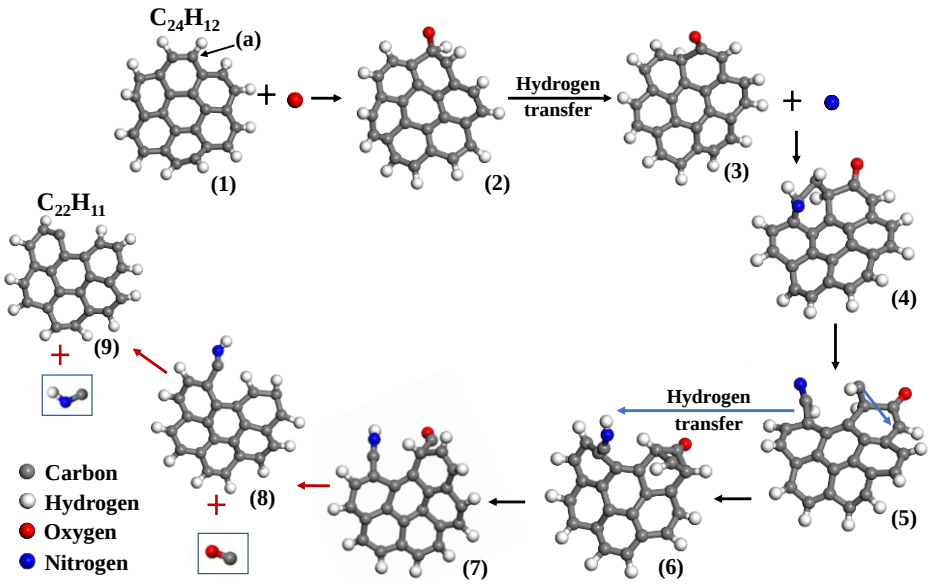

Fig. 12. Evolution of species morphology in the oxidation of $C_{24}H_{12}$.

4 Conclusion

In this study, a series of ReaxFF MD simulations were performed to investigate both the pyrolysis and oxidation with different oxidizers (O_2, NO, NO_2) of coronene at the atomistic scale under high temperature and pressure for the first time. The pyrolysis and oxidation systems are conducted at 2500 K and 50 atm. The largest species found in the pyrolysis system has 95 carbon atoms. The addition of oxidizers inhibits the sooting tendency to various extents. The results show that $C_{75}H_{33}O_2$, $C_{47}H_{24}O$ and $C_{33}H_{11}N_6O_2$ are the largest species in the $C_{24}H_{12}$+O_2, $C_{24}H_{12}$+NO and $C_{24}H_{12}$+NO_2 systems, respectively. The oxidation ability of different oxidizers is closely related to the number of reactive factors including O and N radicals. In the $C_{24}H_{12}$ + O_2 system, the formation of O and OH radicals via O_2 + H → O + OH is limited by the generation of H radicals from dehydrogenation. The oxidation of PAHs by NO_x is more effective than that by O_2. O and N radicals generated in the high-temperature reaction of NO_x are actively involved in the oxidation of PAHs. For O, OH and N radials, H abstraction is a minor pathway with the

addition reaction being a major contributor because of the large molecular size of PAHs. In particular, the presence of NO_2 greatly increases the number of O radicals in the system via the decomposition reaction of NO_2 into NO and O, which significantly accelerates the oxidation of PAHs. The role of NO_x in soot oxidation can be summarized in two steps. First, the O and N radicals add to the PAHs. Note that, the energetically preferable site for O radical attack is the C atom in the outer edge. After that, it successively decomposes to CO_x or (H)CN. This research not only facilitates our understanding of soot oxidation, but also provides new insight into the joint reduction of soot and nitrogen oxides.

Acknowledgements

This work was supported by the National Natural Science Foundation of China (Grant No. 51921004). Qian Mao acknowledges the research fellowship from Alexander von Humboldt Foundation.

References

[1] Q. Chu, C. Wang, D. Chen, Toward full ab initio modeling of soot formation in a nanoreactor, Carbon 199 (2022) 87-95.

[2] Q. Mao, C. Huang, M. Baroncelli, L. Shen, L. Cai, K. Leonhard, H. Pitsch, Unimolecular reactions of the resonance-stabilized cyclopentadienyl radicals and their role in the polycyclic aromatic hydrocarbon formation, Proc. Combust. Inst. 38 (2021) 729-737.

[3] Q. Mao, L. Cai, R. Langer, H. Pitsch, The role of resonance-stabilized radical chain reactions in polycyclic aromatic hydrocarbon growth: Theoretical calculation and kinetic modeling, Proc. Combust. Inst. 38 (2021) 1459-1466.

[4] A. Sharma, K.M. Mukut, S.P. Roy, E. Goudeli, The coalescence of incipient soot clusters, Carbon 180 (2021) 215-225.

[5] C. Irimiea, A. Faccinetto, X. Mercier, I.-K. Ortega, N. Nuns, E. Therssen, P. Desgroux, C. Focsa, Unveiling trends in soot nucleation and growth: When secondary ion mass spectrometry meets statistical analysis, Carbon 144 (2019) 815-830.

[6] D. Hou, L. Pascazio, J. Martin, Y. Zhou, M. Kraft, X. You, On the reactive coagulation of incipient soot nanoparticles, J. Aerosol Sci. 159 (2022) 105866.

[7] H. Kellerer, R. Koch, S. Wittig, Measurements of the growth and coagulation of soot particles in a high-pressure shock tube, Combust. Flame 120 (2000) 188-199.

[8] F. Zhang, C. Wang, W. Han, Y. Zou, J. Wang, S. Seifert, R.E. Winans, Soot formation and growth with palladium acetylacetonate-toluene injection in ethylene base flames investigated by in situ synchrotron small-angle X-ray scattering, Proc. Combust. Inst. 38 (2021) 1859-1866.

[9] A. Wick, A. Attili, F. Bisetti, H. Pitsch, DNS-driven analysis of the Flamelet/Progress Variable model assumptions on soot inception, growth, and oxidation in turbulent flames, Combust. Flame 214 (2020) 437-449.

[10] Y. Liu, X. Zhang, G. Lyu, Y. Qiao, W. Zhang, C. Song, Effect of the oxidation-induced fragmentation of primary particles on soot oxidation reactivity, Combust. Flame 240 (2022) 112026.

[11] G.A. Kelesidis, S.E. Pratsinis, Soot light absorption and refractive index during agglomeration and surface growth, Proc. Combust. Inst. 37 (2019) 1177-1184.

[12] A. Nobili, L. Pratali Maffei, A. Baggioli, M. Pelucchi, A. Cuoci, C. Cavallotti, T. Faravelli, On the radical behavior of large polycyclic aromatic hydrocarbons in soot formation and oxidation, Combust. Flame 235 (2022) 111692.

[13] M. Frenklach, H. Wang, Detailed modeling of soot particle nucleation and growth, Symposium (International) on Combustion 23 (1991) 1559-1566.

[14] Q. Chu, B. Shi, H. Wang, D. Chen, L. Liao, Hydrogen abstraction/addition reactions in soot surface growth, Phys. Chem. Chem. Phys. 23 (2021) 3071-3086.

[15] Y. Wang, S.H. Chung, Soot formation in laminar counterflow flames, Prog. Energy Combust. Sci. 74 (2019) 152-238.

[16] M. Zhang, J.C. Ong, K.M. Pang, X.-S. Bai, J.H. Walther, Large eddy simulation of soot formation and oxidation for different ambient temperatures and oxygen levels, Appl. Energy 306 (2022) 118094.

[17] X. Mao, S. Liu, W. Liu, X. Wu, S. Liu, A simple model catalyst study to distinguish the roles of different oxygen species in propane and soot combustion, Appl. Catal., B 310 (2022) 121331.

[18] F. Dulieu, S. Morisset, A.-S.I. Mohamed, L. Boshman, S. Cazaux, D. Teillet-Billy, S. Baouche, N. Rougeau, Reactivity of coronene with O-atoms, a possible route to ketene in the interstellar medium, Mol. Astrophysics 17 (2019) 100054.

[19] A. Raj, G.R. da Silva, S.H. Chung, Reaction mechanism for the free-edge oxidation of soot by O2, Combust. Flame 159 (2012) 3423-3436.

[20] M. Schejbal, J. Štěpánek, M. Marek, P. Kočí, M. Kubíček, Modelling of soot oxidation by NO2 in various types of diesel particulate filters, Fuel 89 (2010) 2365-2375.

[21] I.P. Kandylas, O.A. Haralampous, G.C. Koltsakis, Diesel soot oxidation with NO2: engine experiments and simulations, Ind. Eng. Chem. Res. 41 (2002) 5372-5384.

[22] P. Ehrburger, J.-F. Brilhac, Y. Drouillot, V. Logie, P. Gilot, Reactivity of soot with nitrogen oxides in exhaust stream, Report No. 0148-7191, SAE Technical Paper, 2002.

[23] M. Jeguirim, V. Tschamber, J.F. Brilhac, P. Ehrburger, Interaction mechanism of NO2 with carbon black: effect of surface oxygen complexes, J. Anal. Appl. Pyrolysis 72 (2004) 171-181.

[24] C. Tighe, M. Twigg, A. Hayhurst, J. Dennis, The kinetics of oxidation of diesel soots by NO2, Combust. Flame 159 (2012) 77-90.

[25] Y. Ren, S. Li, Y. Zhang, D.T. Stephen, M.B. Long, Absorption-ablation-excitation mechanism of laser-cluster interactions in a nanoaerosol system, Phys. Rev. Lett. 114 (2015) 093401.

[26] Z. Li, W. Zhang, Z. Chen, Q. Jiang, Mechanism of accelerating soot oxidation by NO2 from diesel engine exhaust, Environ. Pollut. 264 (2020) 114708.

[27] M. Abián, E. Peribáñez, Á. Millera, R. Bilbao, M.U. Alzueta, Impact of nitrogen oxides (NO, NO2, N2O) on the formation of soot, Combust. Flame 161 (2014) 280-287.

[28] J.E. Dec, A conceptual model of DL diesel combustion based on laser-sheet imaging, SAE transactions, (1997) 1319-1348.

[29] B.R. Stanmore, J.-F. Brilhac, P. Gilot, The oxidation of soot: a review of experiments, mechanisms and models, carbon 39 (2001) 2247-2268.

[30] J.B. Heywood, Internal combustion engine fundamentals, McGraw-Hill Education2018.

[31] Q. Mao, K.H. Luo, Trace metal assisted polycyclic aromatic hydrocarbons fragmentation, growth and soot nucleation, Proc. Combust. Inst. 37 (2019) 1023-1030.

[32] Q. Mao, Y. Ren, K. Luo, A.C. Van Duin, Dynamics and kinetics of reversible homo-molecular dimerization of polycyclic aromatic hydrocarbons, J. Chem. Phys. 147 (2017) 244305.

[33] N. Orekhov, G. Ostroumova, V. Stegailov, High temperature pure carbon nanoparticle formation: Validation of AIREBO and ReaxFF reactive molecular dynamics, Carbon 170 (2020) 606-620.

[34] H. Kwon, S. Shabnam, A.C.T. van Duin, Y. Xuan, Numerical simulations of yield-based sooting tendencies of aromatic fuels using ReaxFF molecular dynamics, Fuel 262 (2020) 116545.

[35] Q.-D. Wang, J.-B. Wang, J.-Q. Li, N.-X. Tan, X.-Y. Li, Reactive molecular dynamics simulation and chemical kinetic modeling of pyrolysis and combustion of n-dodecane, Combust. Flame 158 (2011) 217-226.

[36] J.E. Mueller, A.C. Van Duin, W.A. Goddard III, Application of the ReaxFF reactive force field to reactive dynamics of hydrocarbon chemisorption and decomposition, J. Phys. Chem. C 114 (2010) 5675-5685.

[37] J. Tersoff, New empirical approach for the structure and energy of covalent systems, Phys. Rev. B 37 (1988) 6991.

[38] D.W. Brenner, O.A. Shenderova, J.A. Harrison, S.J. Stuart, B. Ni, S.B. Sinnott, A second-generation reactive empirical bond order (REBO) potential energy expression for hydrocarbons, J. Phys.: Condens. Matter 14 (2002) 783.

[39] N. Nayir, M.Y. Sengul, A.L. Costine, P. Reinke, S. Rajabpour, A. Bansal, A. Kozhakhmetov, J. Robinson, J.M. Redwing, A. van Duin, Atomic-scale probing of defect-assisted Ga intercalation through graphene using ReaxFF molecular dynamics simulations, Carbon 190 (2022) 276-290.

[40] X.Z. Jiang, K.H. Luo, Reactive and electron force field molecular dynamics simulations of electric field assisted ethanol oxidation reactions, Proc. Combust. Inst. 38 (2021) 6605-6613.

[41] A.C. Van Duin, S. Dasgupta, F. Lorant, W.A. Goddard, ReaxFF: a reactive force field for hydrocarbons, J. Phys. Chem. A 105 (2001) 9396-9409.

[42] T.P. Senftle, S. Hong, M.M. Islam, S.B. Kylasa, Y. Zheng, Y.K. Shin, C. Junkermeier, R. Engel-Herbert, M.J. Janik, H.M. Aktulga, T. Verstraelen, A. Grama, A.C.T. Van Duin, The ReaxFF reactive force-field: Development, applications and future directions, npj Comput. Mater. 2 (2016).

[43] K. Chenoweth, A.C. Van Duin, W.A. Goddard, ReaxFF reactive force field for molecular dynamics simulations of hydrocarbon oxidation, J. Phys. Chem. A 112 (2008) 1040-1053.

[44] C. Ashraf, A.C. Van Duin, Extension of the ReaxFF combustion force field toward syngas combustion and initial oxidation kinetics, J. Phys. Chem. A 121 (2017) 1051-1068.

[45] M. Kowalik, C. Ashraf, B. Damirchi, D. Akbarian, S. Rajabpour, A.C. Van Duin, Atomistic scale analysis of the carbonization process for C/H/O/N-based polymers with the ReaxFF reactive force field, J. Phys. Chem. B 123 (2019) 5357-5367.

[46] M. Zheng, X. Li, L. Guo, Investigation of N behavior during coal pyrolysis and oxidation using ReaxFF molecular dynamics, Fuel 233 (2018) 867-876.

[47] C. Barckholtz, T.A. Barckholtz, C.M. Hadad, C− H and N− H bond dissociation energies of small aromatic hydrocarbons, J. Am. Chem. Soc. 121 (1999) 491-500.

[48] Q. Mao, L. Cai, H. Pitsch, Theoretical analysis and kinetic modeling of hydrogen abstraction and addition of 1, 3-cyclopentadiene and associated reactions on the C5H7 potential energy surface, Combust. Flame 222 (2020) 423-433.

[49] R.D. Bach, H.B. Schlegel, The bond dissociation energy of the N-O bond, J. Phys. Chem. A 125 (2021) 5014-5021.

[50] H.M. Aktulga, J.C. Fogarty, S.A. Pandit, A.Y. Grama, Parallel reactive molecular dynamics: Numerical methods and algorithmic techniques, Parallel Comput. 38 (2012) 245-259.

[51] A. Raj, M. Sander, V. Janardhanan, M. Kraft, A study on the coagulation of polycyclic aromatic hydrocarbon clusters to determine their collision efficiency, Combust. Flame 157 (2010) 523-534.

[52] B. Shukla, M. Koshi, Comparative study on the growth mechanisms of PAHs, Combust. Flame 158 (2011) 369-375.

[53] C. Ao, S. Ruan, W. He, Y. Liu, C. He, K. Xu, L. Zhang, Toward high-level theoretical studies on the reaction kinetics of PAHs growth based on HACA pathway: An ONIOM[G3(MP2,CC)//B3LYP:DFT] method developed, Fuel 301 (2021) 121052.

[54] A.M. Kamat, A.C. Van Duin, A. Yakovlev, Molecular dynamics simulations of laser-induced incandescence of soot using an extended ReaxFF reactive force field, J. Phys. Chem. A 114 (2010) 12561-12572.

[55] M. Feng, X.Z. Jiang, Q. Mao, K.H. Luo, P. Hellier, Initiation mechanisms of enhanced pyrolysis and oxidation of JP-10 (exo-tetrahydrodicyclopentadiene) on functionalized graphene sheets: Insights from ReaxFF molecular dynamics simulations, Fuel 254 (2019) 115643.

[56] M. Feng, X.Z. Jiang, K.H. Luo, A reactive molecular dynamics simulation study of methane oxidation assisted by platinum/graphene-based catalysts, Proc. Combust. Inst. 37 (2019) 5473-5480.

[57] M. Döntgen, M.-D. Przybylski-Freund, L.C. Kröger, W.A. Kopp, A.E. Ismail, K. Leonhard, Automated discovery of reaction pathways, rate constants, and transition states using reactive molecular dynamics simulations, J. Chem. Theory Comput. 11 (2015) 2517-2524.

[58] S. Deng, M.E. Mueller, Q.N. Chan, N.H. Qamar, B.B. Dally, Z.T. Alwahabi, G.J. Nathan, Hydrodynamic and chemical effects of hydrogen addition on soot evolution in turbulent nonpremixed bluff body ethylene flames, Proc. Combust. Inst. 36 (2017) 807-814.

[59] T.G. Benish, A.L. Lafeur, K. Taghiadeh, J.B. Howard, C2H2 and PAH as soot growth reactants in premixed C2H4-air flames, Symposium (International) on Combustion 26 (1996) 2319-2326.

[60] Q. Mao, A.C.T. van Duin, K.H. Luo, Formation of incipient soot particles from polycyclic aromatic hydrocarbons: A ReaxFF molecular dynamics study, Carbon 121 (2017) 380-388.

[61] A. Raj, M. Celnik, R. Shirley, M. Sander, R. Patterson, R. West, M. Kraft, A statistical approach to develop a detailed soot growth model using PAH characteristics, Combust. Flame 156 (2009) 896-913.

[62] A. Raj, P.L. Man, T.S. Totton, M. Sander, R.A. Shirley, M. Kraft, New polycyclic aromatic hydrocarbon (PAH) surface processes to improve the model prediction of the composition of combustion-generated PAHs and soot, Carbon 48 (2010) 319-332.

[63] F. Zasada, W. Piskorz, P. Stelmachowski, P. Legutko, A. Kotarba, Z. Sojka, Density functional theory modeling and time-of-flight secondary ion mass spectrometric and X-ray photoelectron spectroscopic investigations into mechanistic key events of coronene oxidation: toward molecular understanding of soot combustion, J. Phys. Chem. C 119 (2015) 6568-6580.

[64] R. Ananthula, T. Yamada, P.H. Taylor, Kinetics of OH radical reaction with anthracene and anthracene-d 10, J. Phys. Chem. A 110 (2006) 3559-3566.

[65] Q. Wu, M. Jing, Y. Wei, Z. Zhao, X. Zhang, J. Xiong, J. Liu, W. Song, J. Li, High-efficient catalysts of core-shell structured Pt@ transition metal oxides (TMOs) supported on 3DOM-Al2O3 for soot oxidation: The effect of strong Pt-TMO interaction, Appl. Catal., B 244 (2019) 628-640.

[66] Z. Xu, C.-H. Hsu, M.-C. Lin, Ab initio kinetics of the reaction of HCO with NO: Abstraction versus association/elimination mechanism, J. Chem. Phys. 122 (2005) 234308.

[67] J. Rodriguez-Mirasol, A.C. Ooms, J.R. Pels, F. Kapteijn, J.A. Moulijn, NO and N2O decomposition over coal char at fluidized-bed combustion conditions, Combust. Flame 99 (1994) 499-507.

[68] C.-H. Chin, T. Zhu, J.Z.H. Zhang, Cyclopentadienyl radical formation from the reaction of excited nitrogen atoms with benzene: a theoretical study, Phys. Chem. Chem. Phys. 23 (2021) 12408-12420.

Table captions

Table 1 Bond dissociation energies of NO_2 and NO with quantum chemistry methods and the ReaxFF Force Field (Unit: kcal/mol)

Table 2 Simulation conditions of $C_{24}H_{12}$ pyrolysis and oxidation.

Table 1. Bond dissociation energies of NO_2 and NO with quantum chemistry methods and the ReaxFF Force Field (Unit: kcal/mol)

	CBS-QB3	ReaxFF	ReaxFF deviation from CBS-QB3	
			absolute difference	relative difference (%)
NO_2	74.20	73.43	0.77	1.03
NO	151.68	160.65	8.91	5.87

Table 2 Simulation conditions of $C_{24}H_{12}$ pyrolysis and oxidation.

System	Molecules	Temperature (K)	Pressure (atm)
$C_{24}H_{12}$	$100C_{24}H_{12}+2700Ar$	2500	50
$C_{24}H_{12}+O_2$	$100C_{24}H_{12}+1350O_2+1350Ar$		
$C_{24}H_{12}+NO$	$100C_{24}H_{12}+1350NO+1350Ar$		
$C_{24}H_{12}+NO_2$	$100C_{24}H_{12}+1350NO_2+1350Ar$		

Figure captions

Fig. 1. Time evolution of the C_6H_6/C_5H_6 molecule number for systems with different oxidizers utilizing (a) CHON-2019 and (b) CHONS-2012.

Fig. 2. Time evolution of the $C_{24}H_{12}$ molecule number in systems under pyrolysis and oxidation conditions with different oxidizers (O_2, NO, NO_2) at 2500 K.

Fig. 3. Proportion of the main first-step reactions of $C_{24}H_{12}$ in systems under pyrolysis and oxidation conditions with different oxidizers (O_2, NO, NO_2) at 2500 K.

Fig. 4. Time evolution of the number of molecules with different carbon numbers in the $C_{24}H_{12}$ pyrolysis system.

Fig. 5. Time evolution of the number of molecules with different carbon numbers in the $C_{24}H_{12}+O_2$ system.

Fig. 6. Reaction pathways of $C_{24}H_{12}$ oxidation by O_2. The number of reactions is indicated in red.

Fig. 7. Time evolution of the number of molecules with different carbon numbers in the systems of (a) $C_{24}H_{12}$+NO, and (b) $C_{24}H_{12}+NO_2$.

Fig. 8. Reaction pathways of the NO system and the $C_{24}H_{12}$+NO system. The numbers of reactions in the NO system and the $C_{24}H_{12}$+NO system are indicated in blue and red, respectively. The dashed lines indicate the processes that are only discovered in the pure NO system.

Fig. 9. Time evolution of the molecular numbers of NO, N_2, N, and O in the $C_{24}H_{12}$+NO system before 1200 ps. The arrows on the right side show the number of NO, N_2, N, and O at 1200 ps in the pure NO system.

Fig. 10. Reaction pathways of the pure NO_2 system and the $C_{24}H_{12}+NO_2$ system. The numbers of reactions in the NO_2 system and the $C_{24}H_{12}+NO_2$ system are indicated in blue and red, respectively. Dashed lines indicate that the processes are only discovered in the pure NO_2 system.

Fig. 11. Time evolution of the molecule number of NO_2, NO, N_2, O_2, N, and O in the $C_{24}H_{12}$+NO_2 system before 1200 ps. The arrows on the left side show the number of NO_2, NO, N_2, O_2, N, and O at 1200 ps in the pure NO_2 system.

Fig. 12. Evolution of species morphology in the oxidation of $C_{24}H_{12}$.

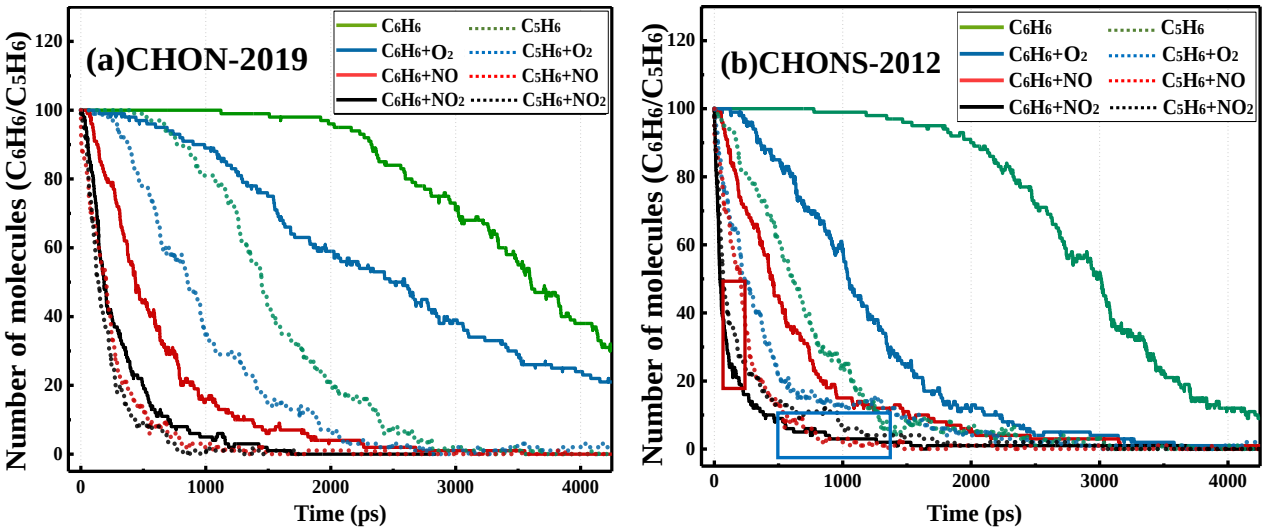

Fig. 1. Time evolution of the C_6H_6/C_5H_6 molecule number for systems with different oxidizers utilizing (a) CHON-2019 and (b) CHONS-2012.

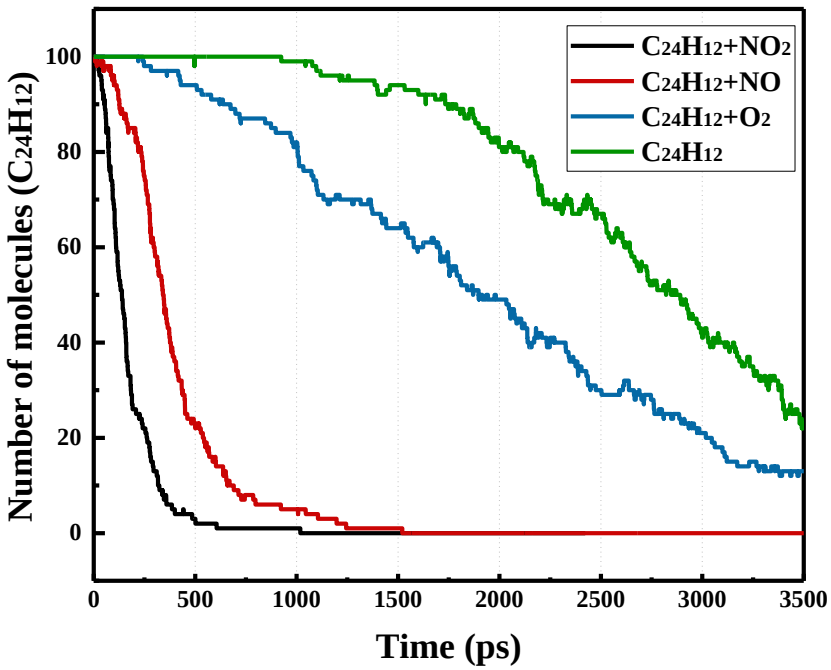

Fig. 2. Time evolution of the $C_{24}H_{12}$ molecule number in systems under pyrolysis and oxidation conditions with different oxidizers (O_2, NO, NO_2) at 2500 K.

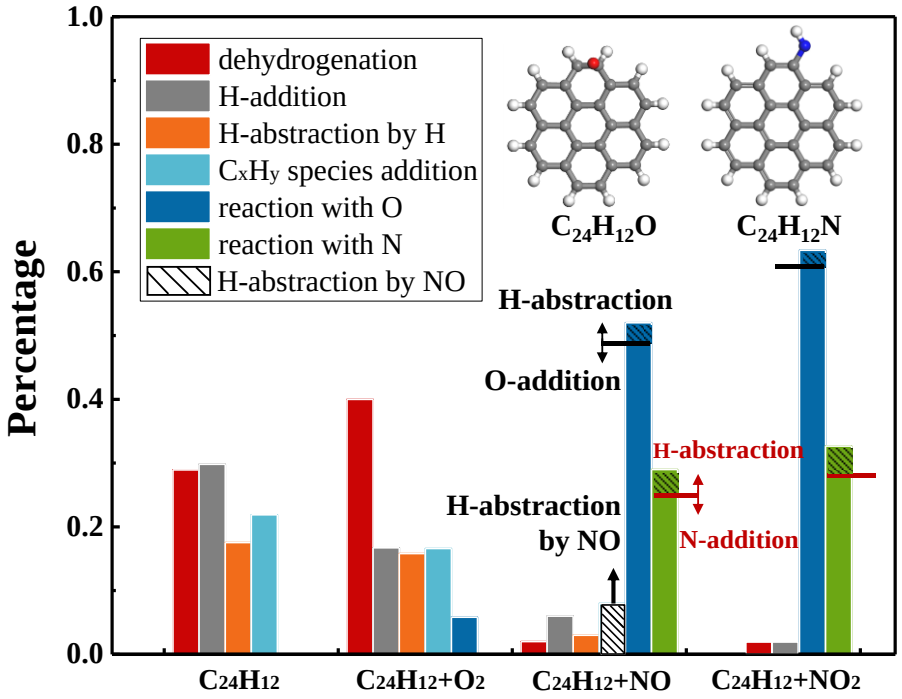

Fig. 3. Proportion of the main first-step reactions of $C_{24}H_{12}$ in systems under pyrolysis and oxidation conditions with different oxidizers (O_2, NO, NO_2) at 2500 K.

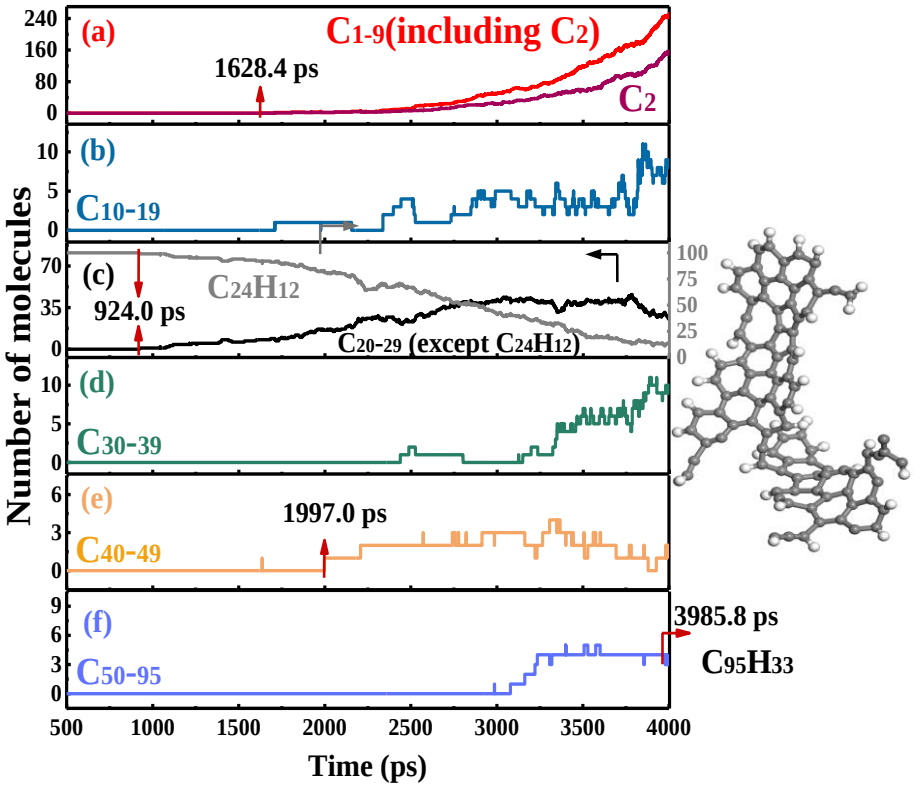

Fig. 4. Time evolution of the number of molecules with different carbon numbers in the $C_{24}H_{12}$ pyrolysis system.

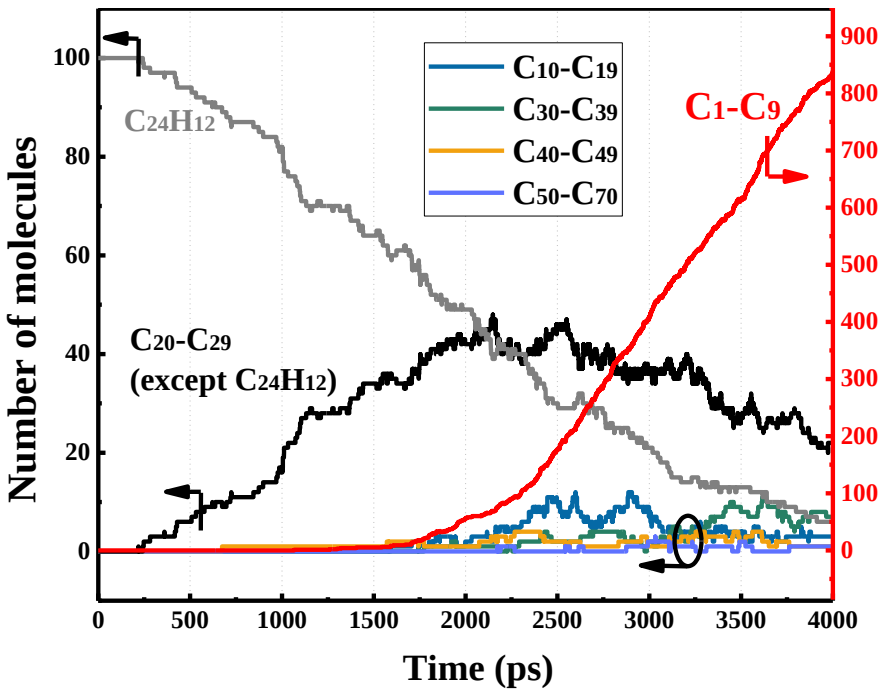

Fig. 5. Time evolution of the number of molecules with different carbon numbers in the $C_{24}H_{12}$+O_2 system.

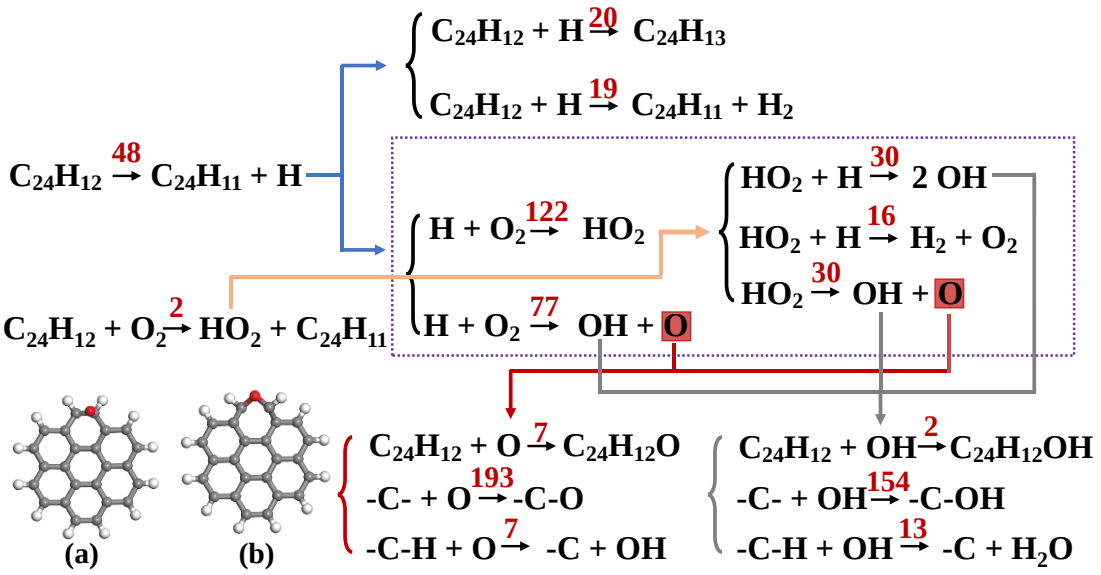

Fig. 6. Reaction pathways of $C_{24}H_{12}$ oxidation by O_2. The number of reactions is indicated in red.

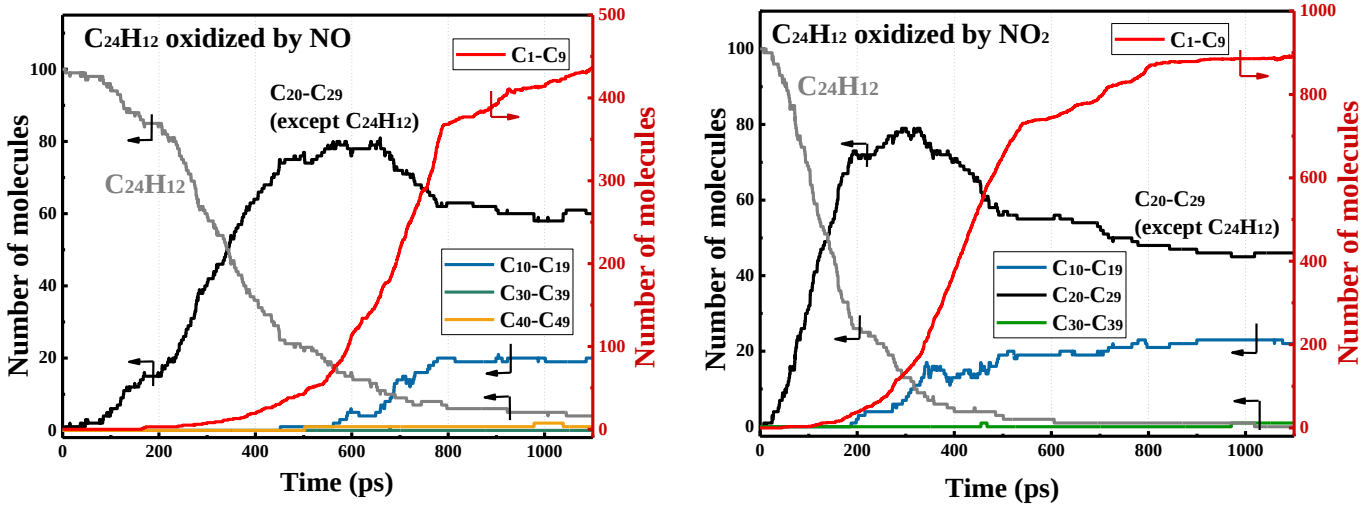

(a) **(b)**

Fig. 7. Time evolution of the number of molecules with different carbon numbers in the systems of (a) $C_{24}H_{12}$+NO, and (b) $C_{24}H_{12}$+NO_2.

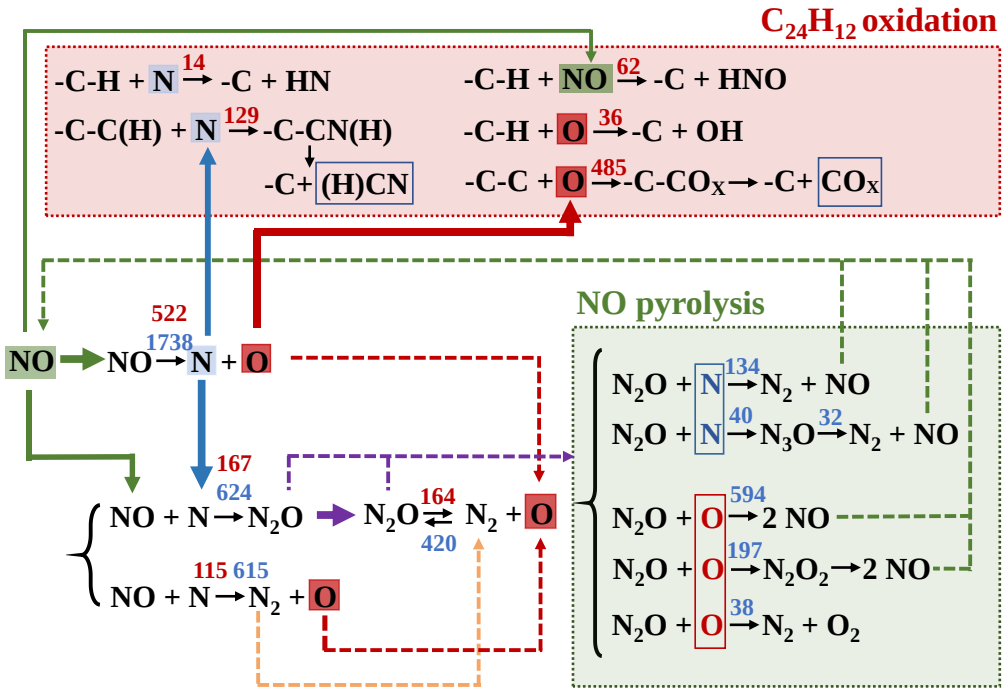

Fig. 8. Reaction pathways of the NO system and the $C_{24}H_{12}$+NO system. The numbers of reactions in the NO system and the $C_{24}H_{12}$+NO system are indicated in blue and red, respectively. The dashed lines indicate the processes that are only discovered in the pure NO system.

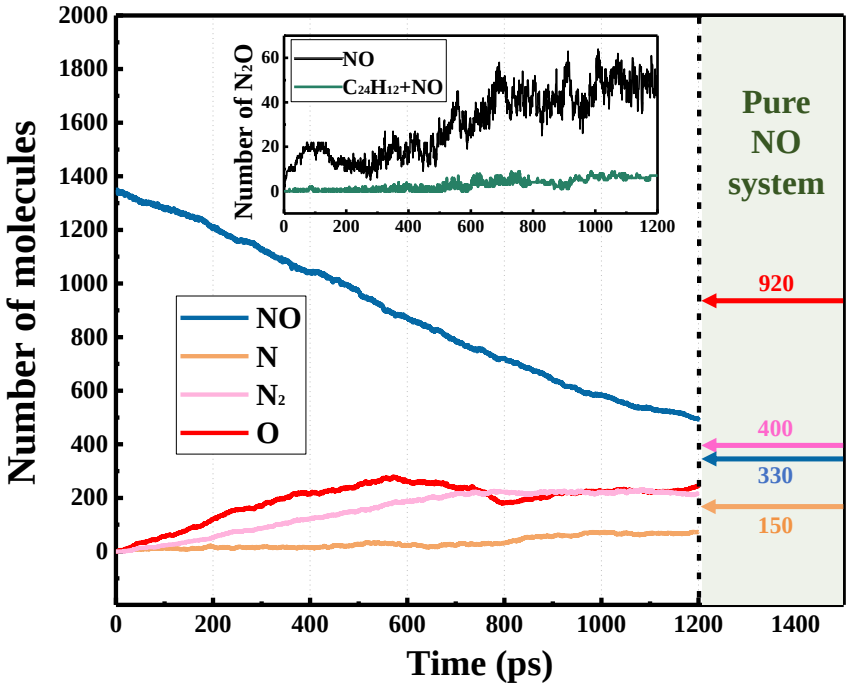

Fig. 9. Time evolution of the molecular numbers of NO, N_2, N, and O in the $C_{24}H_{12}$+NO system before 1200 ps. The arrows on the right side show the number of NO, N_2, N, and O at 1200 ps in the pure NO system.

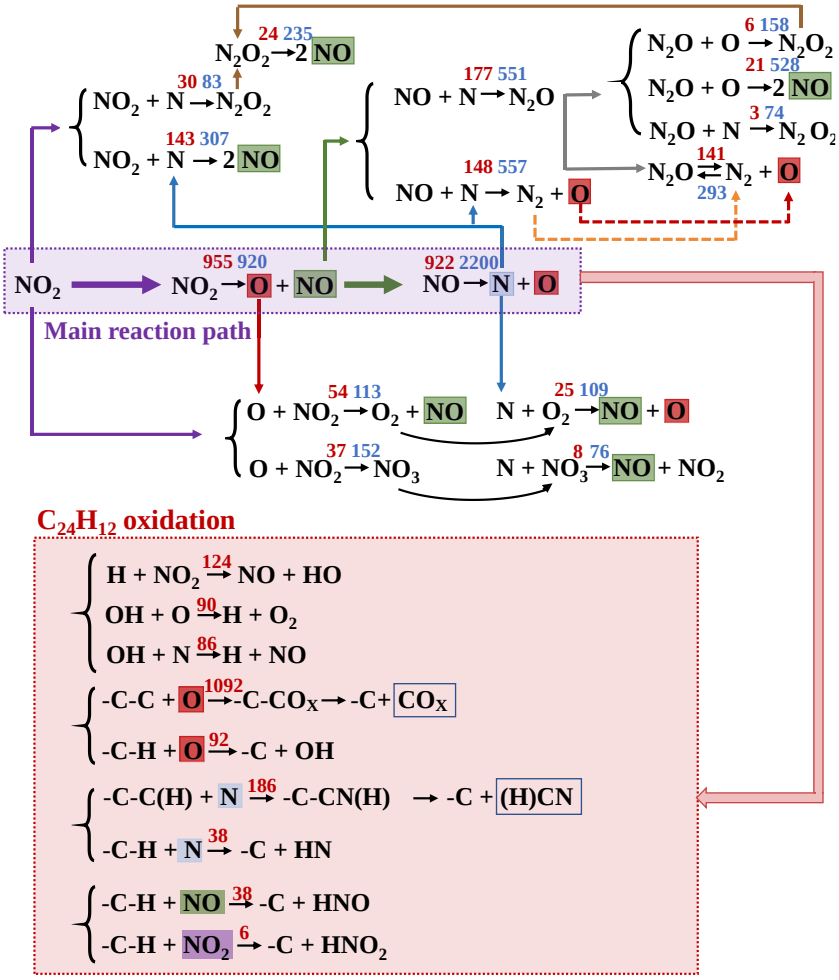

Fig. 10. Reaction pathways of the pure NO_2 system and the $C_{24}H_{12}$+NO_2 system. The numbers of reactions in the NO_2 system and the $C_{24}H_{12}$+NO_2 system are indicated in blue and red, respectively. Dashed lines indicate that the processes are only discovered in the pure NO_2 system.

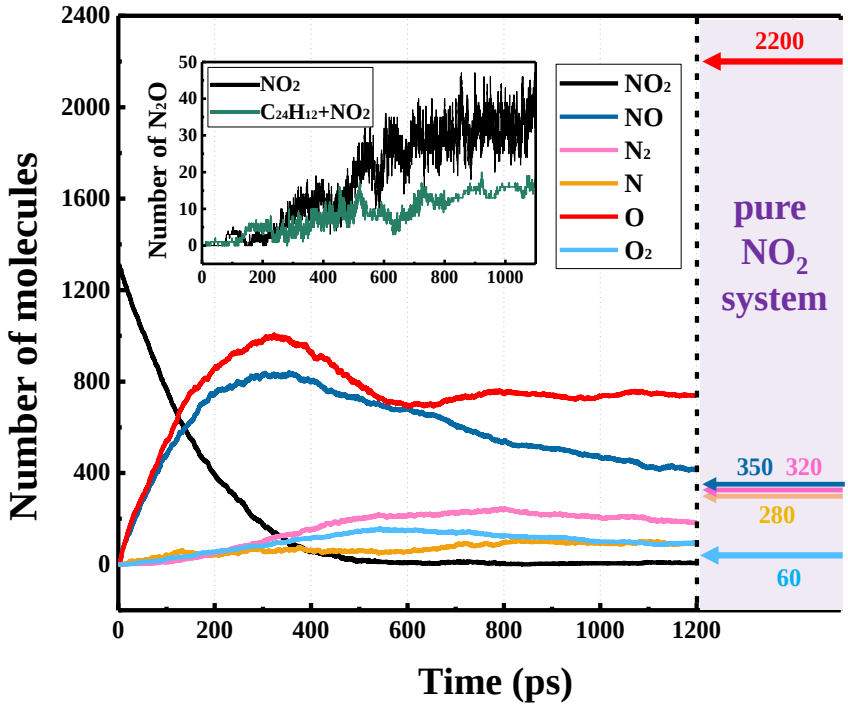

Fig. 11. Time evolution of the molecule number of NO_2, NO, N_2, O_2, N, and O in the $C_{24}H_{12}$+NO_2 system before 1200 ps. The arrows on the left side show the number of NO_2, NO, N_2, O_2, N, and O at 1200 ps in the pure NO_2 system.

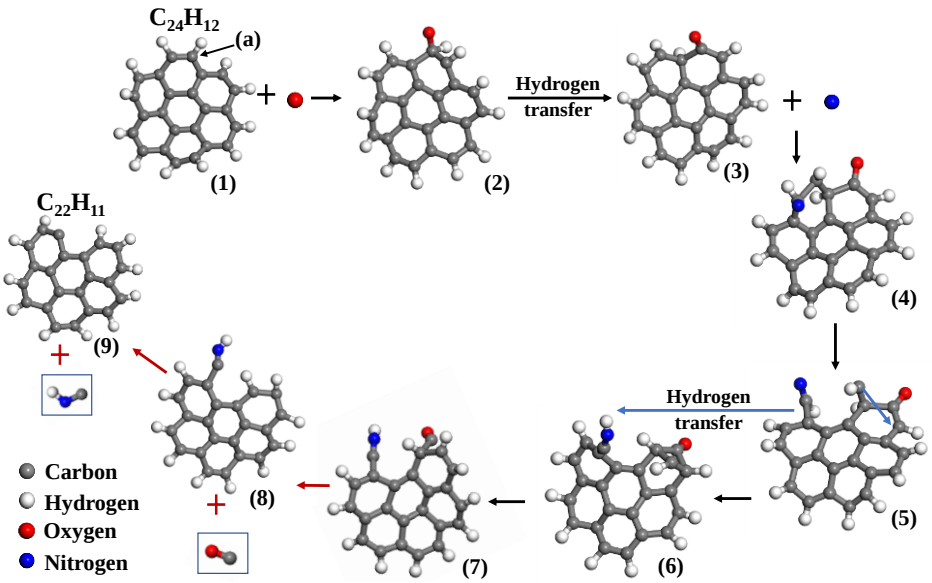

Fig. 12. Evolution of species morphology in the oxidation of $C_{24}H_{12}$.

Declaration of interests

☒ The authors declare that they have no known competing financial interests or personal relationships that could have appeared to influence the work reported in this paper.

☐The authors declare the following financial interests/personal relationships which may be considered as potential competing interests: